Available online at www.sciencedirect.com
SCIENCE DIRECT®
Ecological Modelling 188 (2005) 217–252
ECOLOGICAL MODELLING
www.elsevier.com/locate/ecolmodel

Intercomparison of techniques to model high temperature effects on CO_2 and energy exchange in temperate and boreal coniferous forests

R.F. Grant [a,*], A. Arain [b], V. Arora [c], A. Barr [d], T.A. Black [e], J. Chen [f], S. Wang [g], F. Yuan [b], Y. Zhang [g]

[a] *Department of Renewable Resources, University of Alberta, Edmonton, Alta., Canada T6G 2E3*
[b] *School of Geography and Geology, McMaster University, Hamilton, Ont., Canada*
[c] *Environment Canada, Victoria, BC, Canada*
[d] *Environment Canada, Saskatoon, Sask., Canada*
[e] *Department of Soil Science, University of British Columbia, Vancouver, BC, Canada*
[f] *Department of Geography, University of Toronto, Toronto, Ont., Canada*
[g] *Canadian Centre for Remote Sensing, Ottawa, Ont., Canada*

Received 4 August 2004; received in revised form 21 January 2005; accepted 31 January 2005
Available online 23 May 2005

Abstract

The increased frequency of high atmospheric temperatures (T_a) predicted under current climate change scenarios may adversely impact net ecosystem productivity (*NEP*) of temperate and boreal conifers. The ability to simulate CO_2 and energy exchange under contrasting T_a and vapor pressure deficit (D) is therefore an important attribute in models used to predict climate change impacts on conifer *NEP*. We tested six ecosystem models differing in their approach to the simulation of T_a and D effects on CO_2 and energy exchange against eddy covariance fluxes recorded under changing T_a and D over a temperate Douglas fir stand and a boreal jack pine stand. These stands changed from sinks to sources of CO_2 whenever T_a and D rose above 25 °C and 2.5 kPa. The extent to which the models were able to simulate these changes depended on their ability to simulate (1) lower stomatal conductance (g_l) and hence earlier midday declines in CO_2 influxes under higher D, and (2) rising autotrophic (R_a) and heterotrophic (R_h) respiration under rising T_a. Most of the models in this study accurately simulated the net gain of C by conifers under low T_a and D, but underestimated the net loss of C by conifers under high T_a and D. This underestimation was attributed to an inadequate sensitivity of g_l to D and of R_a and R_h to temperature in some of the models. Differences in CO_2 fluxes modelled at hourly time scales were associated with large differences in annual gross and net primary productivities modelled at annual time scales, indicating the importance of accurately modelling these fluxes. The ability to distinguish among alternative algorithms for their accuracy in calculating CO_2 and energy fluxes was often limited by uncertainty in the measurement of these fluxes

* Corresponding author. Tel.: +1 403 492 4413; fax: +1 403 492 1767.
E-mail address: robert.grant@ualberta.ca (R.F. Grant).

0304-3800/$ – see front matter © 2005 Published by Elsevier B.V.
doi:10.1016/j.ecolmodel.2005.01.060

using eddy covariance, especially when low wind speeds and stable boundary layers reduced atmospheric turbulence. Further progress in model testing will require that this uncertainty be more clearly established and reduced.

Keywords: CO_2 exchange; Energy exchange; Ecosystem modelling; Eddy covariance; Coniferous forests; High temperature effects

1. Introduction

High atmospheric temperatures (T_a) have been shown to impact adversely the net ecosystem productivity (*NEP*) of temperate and boreal conifers. Morgenstern et al. (2004a) found that high T_a during an El Niño event reduced *NEP* of a temperate coastal Douglas fir stand by raising ecosystem respiration (R_e) more than gross primary productivity (*GPP*). Griffis et al. (2003) found that boreal conifers experienced a pronounced mid-season decline in *NEP* due to larger R_e and reduced *GPP*. Grant et al. (2001a) showed that boreal black spruce changed from a sink to a source of CO_2 as daily maximum/minimum temperature rose above 25/15 °C. These impacts on *NEP* occurred because *GPP* did not rise, and may even have declined, under higher T_a, while both autotrophic and heterotrophic respiration (R_a and R_h) rose exponentially with temperature.

The sensitivity of *GPP* to high T_a in boreal conifers may be biochemical or stomatal in origin. Méthy et al. (1997) found degradation of PSII photochemical efficiency in *Pinus halapensis* only at temperatures >35 °C which is well above those at which *GPP* becomes constrained. However stomatal conductance (g_l) of boreal conifers has been frequently observed to decline under higher atmospheric vapor pressure deficits (*D*) (Grelle et al., 1999; Ohta et al., 2001; Saugier et al., 1997) that can occur when temperatures exceed 25 °C. Declines in g_l are apparent in the larger Bowen ratios measured over boreal conifers under higher temperatures (Jarvis et al., 1997). Lower g_l caused by higher *D* may also constrain CO_2 uptake in conifers. These declines are likely to have a direct impact on *GPP* by constraining CO_2 diffusion into leaves. Kloeppel et al. (2000) found that CO_2 fixation by coniferous needles varied negatively with *D* when $D > 1$ kPa. Law et al. (2000a) found that *NEP* of ponderosa pine approached zero when *D* rose to 2–4 kPa.

The sensitivity of mass and energy exchange to *D* in conifers may be caused by their hydraulic structure. Gao et al. (2002) found that transpiration in pines was several times more sensitive to *D* than was that in broadleaf trees, even though g_l of pines declined less with water potential than that of broadleaf trees due to the structure and composition of their guard cells. They attributed the sensitivity of transpiration in pines to lower xylem hydraulic conductance caused by the tracheid cells from which their xylem is constructed. Lower xylem conductance was hypothesized to force larger soil–canopy water potential gradients and hence lower canopy water potentials (ψ_c) that reduced g_l under high transpiration demand. Pre-dawn ψ_c of conifers has been found to be lower than that of deciduous shrubs, due to incomplete overnight recharge of plant water caused by low xylem conductance (Royce and Barbour, 2001). Menuccini and Grace (1996) reported that low xylem conductance may limit primary productivity in mature pine stands.

The ability to simulate the sensitivity of mass and energy exchange to T_a and *D* is an important attribute in land surface models used to predict climate change impacts on boreal conifer *NEP*. This ability requires the accurate modelling of atmospheric effects on g_l, either from empirical functions of photosynthetically active radiation (PAR), T_a, *D*, soil water potential (ψ_s) (Amthor et al., 1994; Chen et al., 1999; Wullschleger et al., 2003), and atmospheric CO_2 concentration (C_a) (Hunt et al., 1999; Kimball et al., 1997), or from a Ball-Woodrow-Berry function (Ball, 1988) of CO_2 fixation, C_a and *D* (Arain et al., 2002; Baldocchi and Wilson, 2001; King et al., 1997; Nikolov, 1997; Wang and Jarvis, 1990; Wang et al., 2002a,b). In many land surface schemes, this latter function is not explicitly coupled with soil water status, and so requires reparameterization with changing ψ_s (Reichstein et al., 2002). Stomatal conductance can also be calculated directly from CO_2 fixation and ratios of intercellular to atmospheric CO_2 concentrations (C_i:C_a) (Grant, 2001), the conservation of which is the key assumption on which the Ball-Woodrow-Berry function is based. This

sensitivity is best modelled at hourly or sub-hourly time steps, because diurnal effects of D on *NEP* may not be well represented in daily time step models (Law et al., 2000a). Calculation of g_l from C_i:C_a in these models requires the simulation of CO_2 fixation, usually based on Farquhar et al. (1980), through which effects of PAR, T_a and C_a on g_l are mediated.

Temperature effects on boreal *NEP* also include direct effects on CO_2 fixation, R_a and R_h. Those on CO_2 fixation are commonly modelled with Arrhenius functions, key parameters of which are activation energies (typically 50–60 kJ mol^{-1} according to Farquhar et al., 1980), and inactivation energies to account for constraints at low and high temperatures. These functions may be emulated by parabolic or quadratic functions with set temperature optima (e.g. Landsberg and Waring, 1997). Temperature effects on R_a are commonly represented by exponential functions with Q_{10} between 2.0 and 2.5, and those on R_h by Arrhenius or parabolic functions similar to those on CO_2 fixation.

The different modelling hypotheses described above have been subjected to only limited comparative testing against measurements of *NEP* under changing T_a and D in coniferous forests (e.g. Amthor et al., 2001). In this paper, we analyze the ability of six ecosystem models to simulate mass and energy exchange during high T_a events in both temperate and boreal conifers in terms of the hypotheses for T_a effects on which each model is based. This analysis is intended to establish the comparative merits of different modelling hypotheses for high temperature stress and to seek consensus on further development of these hypotheses. The two test sites selected for this analysis are in different climatic zones (temperate Douglas fir – western hemlock and boreal jack pine – black spruce), but both experience high T_a events that are predicted to become more frequent under most climate change scenarios. The models in this intercomparison are those participating the Fluxnet-Canada Research Network (FCRN), the purpose of which is to clarify climate and management effects on *NEP* of Canadian forests.

2. Model descriptions

The six models included in the FCRN all function at time steps of 1 h or less, and so represent the higher end of the range of temporal resolution included in earlier model intercomparisons (e.g. Amthor et al., 2001; Hanson et al., 2004). Although these models were developed for the common purpose of simulating terrestrial *NEP*, differences have emerged in key algorithms and parameters for soil and climate effects on soil–plant–atmosphere mass and energy exchange. The key algorithms and parameters for these effects in the six models are described below with reference to numbered equations in Appendix A.

2.1. Boreal ecosystem productivity simulator (BEPS)

2.1.1. Background

BEPS (Liu et al., 1997; Chen et al., 1999) was developed at the Canadian Centre for Remote Sensing (CCRS) and the University of Toronto for short-term carbon cycle simulations, while the Integrated Terrestrial Ecosystem Carbon Cycle Model (InTEC) (Chen et al., 2000a,b), used here for spin-up of soil carbon, was developed for long-term carbon cycle simulations. These models have been used with remotely sensed estimates of leaf area index (LAI) and land cover, and with Soil Landscapes of Canada (SLC), forest inventory and gridded meteorological data to make regional and national estimates of net primary productivity (*NPP*), *NEP*, and net biome productivity (*NBP*) (Chen et al., 2003).

2.1.2. CO_2 and energy exchange

Because BEPS was designed for efficient remote sensing applications, the full coupling between carbon and nitrogen cycles used in InTEC was not included, so that seasonal soil nutrient dynamics were not simulated in this study. For this reason, a BEPS model version with a fixed maximum photosynthetic capacity (A.1.1) (Leuning, 1990) was used here instead of a later version requiring iterations between stomatal conductance and photosynthetic capacity (Leuning et al., 1995). The effects of canopy temperature (T_c) and the average leaf-level nitrogen (N) content on rubisco-limited CO_2 fixation rate (V_r) (Farquhar et al., 1980) were considered (A.1.2, A.1.3). The effects of T_c (Humphreys et al., 2003), soil moisture (θ) (Bonan, 1991; Zierl, 2001), humidity (Dang et al., 1997), and global radiation on CO_2 and energy fluxes were modelled through their effects on g_l (A.2.1) based on Jarvis (1976). CO_2 fixation rate by the canopy (V_c) was estimated as the sum of those by sunlit and shaded leaves modelled separately

using methods of Chen et al. (1999) with consideration of canopy architecture (A.2.3) (Chen et al., 1997). The total canopy was separated into overstory and understory (Liu et al., 2003). Downward longwave radiation used in energy balance calculations was estimated with an empirical equation. Sensible (*H*) and latent (*LE*) heat fluxes were the sums of those from overstory, understory and moss/soil surfaces modelled separately. The Penman-Monteith equation was used to calculate *LE* from all three layers (A.6.1). Canopy conductance (g_c) was a weighted average of sunlit and shaded leaves for the vegetation layers (A.2.3), while for the moss/soil layer an empirical equation was used that depended on moisture in the top soil layer (Sellers et al., 1996).

2.1.3. Autotrophic respiration and changes in phytomass

R_a was the sum of independently calculated values for maintenance respiration R_m and growth respiration R_g (A.4.1). R_g was a fixed proportion of gross primary productivity (A.4.5), and R_m was divided into leaf, stem and root components as functions of biomass and temperature (A.4.3, A.4.4).

2.1.4. Heterotrophic respiration and changes in SOC

R_h was driven by decomposition of SOC (A.5.1) from nine pools (passive, slow, soil microbe, surface microbe, structural foliage litter, metabolic foliage litter, structural fine root litter, metabolic fine root litter, woody material) (A.5.9, A.5.10) (Parton et al., 1993) in four layers (A.6.7). To model the effects of soil temperature (T_s) and θ on decomposition of these pools (A.5.11, A.5.12), we assumed that litter and surface microbe pools were located in the first layer, while the remaining pools were located in the second and third layers. The sizes of these pools were obtained through a spin-up process using InTEC based on the mean climate and stand age after the model was calibrated against measured soil carbon.

2.2. Ecosys

2.2.1. Background

Ecosys (http://www.ecosys.rr.ualberta.ca/; Grant, 2001) was developed at the University of Alberta as a detailed, comprehensive model of terrestrial ecosystems. It has been used to model climate and land management effects on *NPP* and *NEP* of diverse ecosystems (e.g. Grant, 2003; Grant et al., 2001b, 2003).

2.2.2. Energy exchange

Energy exchanges between the atmosphere and terrestrial surfaces were resolved into those between the atmosphere and the leaf and stem surfaces of each population within the plant community, and that between the atmosphere and each of the surfaces (soil, plant residue, and snow) of the ground beneath (Grant et al., 1999). Energy exchange at ground surfaces was coupled with soil heat and water transfers, including runoff (Manning), infiltration (Green-Ampt), macropore flow (Poiseuille) and micropore flow (Richards) (A.6.5).

Canopy energy exchange was calculated from an hourly two-stage convergence solution for the transfer of water and heat through a multi-layered multi-population soil–root–canopy system. The first stage of this solution required convergence to a value of T_c at which the first-order closure of the canopy energy balance was achieved. During convergence, *LE* between the atmosphere and each plant population was controlled by aerodynamic conductance (g_a) and g_c (A.6.1). Two controlling mechanisms were postulated for g_c:

(1) At the leaf level, a maximum leaf conductance g_{lmax} was calculated for each leaf surface (A.2.1) that allowed a set C_i:C_a ratio for coniferous trees of 0.75 to be maintained at carboxylation rates calculated under ambient irradiance, T_c, C_a and full turgor. Carboxylation was the lesser of CO_2- and light-limited reaction rates (Farquhar et al., 1980) (A.1.13) constrained by product inhibition (Bowes, 1991; Stitt, 1991) (A.1.3, A.1.9), so that both carboxylation rates were fully coupled to rates of product removal. These latter rates were determined by phytomass biosynthesis rates controlled by plant water and nutrient uptake rates (A.6.6, A.3.1). Values of g_{lmax} calculated from C_i:C_a and leaf carboxylation rate were then aggregated by surface area to maximum canopy conductance (g_{cmax}) for use in the energy balance convergence scheme.
(2) At the canopy level, g_c was then reduced from g_{cmax} at full turgor through an exponential function of canopy turgor potential ψ_t (A.2.2) determined from total ψ_c and osmotic ψ_π water potentials

generated during convergence for transpiration versus water uptake (described in Section 2.2.3).

2.2.3. Water uptake

After convergence for T_c, the difference between canopy transpiration E_c from the energy balance (A.6.1) and total water uptake U_r from all rooted layers in the soil (A.6.6) was tested against the difference between canopy water content from the previous hour and that from the current hour. The difference between the two was minimized by adjusting ψ_c used in the next convergence cycle. Hydraulic resistances to U_r in each soil layer were calculated from Poiseuille's law using root radial and axial resistivities derived by Doussan et al. (1998) with root lengths and surface areas from a root system submodel driven by shoot-root C transfers and root C respiration (Grant, 1998a).

2.2.4. CO_2 fixation

After convergence for T_c and ψ_c, carboxylation rates at each leaf surface were adjusted from those calculated under full ψ_t to those under ambient ψ_t (A.1.4). This adjustment was required by the decrease from g_{cmax} (A.2.1) to g_c at ambient ψ_t (A.2.2) during convergence. The adjustment was achieved through a convergence solution for C_i at which the diffusion rate of gaseous CO_2 between C_a and C_i through g_l equalled the carboxylation rate of aqueous CO_2 at the aqueous equivalent of C_i (described in 2.2.2) (A.1.13). This convergence arrived at a lower C_i than that at full ψ_{ti} so that C_i:C_a declined under water stress. The CO_2 fixation rate of each leaf surface at convergence (V_l) was added to arrive at a value for gross canopy CO_2 fixation ($V_c = GPP$).

2.2.5. Autotrophic respiration and changes in phytomass

CO_2 fixation products were added to a nonstructural C pool C_n which was the first-order substrate for R_a (A.4.1, A.4.2). R_a was first used to meet requirements for R_m (A.4.3, A.4.4), then any excess was expended as R_g (A.4.5) to drive biosynthesis according to organ-specific growth yields (A.4.6). If R_a was less than R_m, the shortfall was made up through respiration of remobilizable protein C withdrawn from leaf C (A.4.7), driving the loss of associated structural C as litterfall (A.4.8). Environmental constraints such as nutrient, heat or water stress that reduced C_n and hence R_a with respect to R_m therefore hastened litterfall.

2.2.6. Heterotrophic respiration and changes in SOC

Dissolved organic C (DOC) concentrations drove temperature-dependent (A.5.2) R_h by heterotrophic microbial populations (A.5.1), including obligately aerobic, facultatively anaerobic, obligately anaerobic, and diazotrophic heterotrophic decomposers. These decomposers were associated with each SOC pool, including plant litter (from litterfall in A.4.8), animal manure, particulate organic matter and humus (Grant, 2003). R_h by each population was constrained by rates of electron acceptor (O_2, NO_3^-, NO_2^-, N_2O, organic C) uptake (A.5.3). All microbial populations underwent maintenance respiration R_m (A.5.4, A.5.5) and decomposition. R_h in excess of R_m was used as growth respiration R_g (A.5.6) which drove microbial growth (Grant, 2003) (A.5.7). Active microbial biomass resulting from growth drove temperature-dependent (A.5.2) decomposition of each SOC pool (A.5.8), which was partitioned into components of differing vulnerability to hydrolysis (A.5.9, A.5.10). Decomposition produced DOC which then drove R_h.

2.3. Canadian land surface scheme (CLASS)

2.3.1. Background

CLASS (Verseghy, 2000) was developed by the Meteorological Service of Canada (MSC) for coupling with the Canadian General Circulation Model (CGCM) in regional climate–ecosystem interactions. CLASS has participated in the international Project for Intercomparison of Land-Surface Parameterization Schemes (PILPS).

2.3.2. CO_2 and energy exchange

Versions of the CLASS biospheric component (C-CLASS) are being developed at McMaster University (C-CLASSm) (Arain et al., 2002; Kothavala et al., submitted) and the University of Alberta (C-CLASSa) (Wang et al., 2001, 2002a,b; Zhang et al., 2004). Both versions shared a common approach to the modelling of V_l and g_l. Sunlit leaf area was calculated from light extinction (Wang and Leuning, 1998) accounting for mean foliage projection and canopy clumping following Chen et al. (1997). Shaded leaf area was

considered to be that which was not sunlit (A.2.4). V_l (A.1.1–A.1.13) (Farquhar et al., 1980) and g_l (Ball, 1988) were separately calculated for sunlit and shaded leaves, and then multiplied by sunlit and shaded leaf areas to obtain whole canopy values (A.2.3).

C-CLASSa and C-CLASSm differed in how this basic model of V_l and g_l was coupled with ecosystem C, N and water cycles.

2.4. C-CLASSa

The biospheric component of C-CLASSa consisted of three modules: (1) a water transfer module with calculation schemes for g_l and root conductance, (2) a plant C and N module to simulate V_l, R_a, N uptake, growth, and litterfall, and (3) a soil C and N module to simulate litter and organic matter decomposition and R_h.

2.4.1. Energy exchange and water uptake

The canopy energy balance (Verseghy et al., 1993) was solved concurrently with the canopy water balance (Wang et al., 2002b), by calculating T_c, g_c and ψ_c within a nested convergence scheme. In this scheme, plant transpiration from a first order closure of the canopy energy balance (A.6.1) was equilibrated with root water uptake along a soil–root–canopy ψ gradient (A.6.6). T_c and ψ_c were used in the plant module to determine temperature and water impacts on plant C and N cycling. V_l (A.1.13) used to calculate g_c (A.2.1) was reduced by ψ_c (A.1.4) and shoot non-structural N to C ratio (A.1.3).

2.4.2. Autotrophic respiration and changes in phytomass

V_l supplied C_n (non-structural C) which was the substrate for R_a (A.4.1), some of which sustained R_m calculated from structural N (A.4.3) and a Q_{10} temperature function (A.4.4). R_a in excess of R_m was allocated to R_g (A.4.5) which drove growth of structural C according to organ-specific yield coefficients (A.4.6). Leaf structural C drove LAI through a value for specific leaf area. If R_a was less than R_m, the shortfall was remobilized from structural C (A.4.7), driving litterfall (A.4.8). Additional litterfall caused by plant aging was simulated with first order kinetics. Direct loss of C_n occurred as root exudation, assumed to be proportional to root C_n concentration. C_n and non-structural N pools (N_n) were redistributed between shoot and root according to their concentration gradients. N_n was supplied by root N uptake (A.3.1) constrained by soil mineral N concentration (A.3.2) and plant N_n concentration (A.3.4). Further descriptions of plant C and N processes in C-CLASSa can be found in Wang et al. (2001) and Zhang et al. (2004).

2.4.3. Heterotrophic respiration and changes in SOC

Plant litter and soil organic matter (SOM) were separated into one surface litter layer and the three soil layers used in CLASS (A.6.7). Litterfall from foliage and stem (A.4.8) contributed to the surface litter pool and litterfall from plant roots (A.4.8) and root exudation contributed to the soil litter pools. Litter and SOM pools were each further divided into three C and N fractions with differing resistance to decomposition, calculated as a first-order function of each pool (A.5.8) with fraction-specific rate coefficients (A.5.9, A.5.10). Also represented in each layer were microbial C and N pools, the latter of which exchanged N with a mineral N pool according to microbial C:N ratios. Mineral N pools were also the source of root N uptake (A.3.2). The decomposition of all litter and SOM pools depended on T_s (A.5.11), ψ_s (A.5.12) and dissolved organic C:N ratio (A.5.8). The fraction of decomposed litter or SOC incorporated into microbial biomass was set from pool-specific yield efficiencies, and the remainder was allocated to R_h (A.5.1). Wet deposition and leaching of N were also modelled. Details of soil C and N cycling processes were presented in Wang et al. (2002a).

2.5. C-CLASSm

The biospheric component of C-CLASSm consisted of two modules: (1) a plant C module to simulate g_c and photosynthesis, which was sensitive to foliar N status and (2) a carbon budgeting module which allocated C sequestered to three live vegetation pools, calculated R_a, litter and organic matter decomposition and R_h.

2.5.1. CO_2 and energy exchange

In C-CLASSm, g_c for water vapor, calculated as 1.56 times of that for CO_2, was sensitive to soil water availability (through f_w in A.1.4), V_l (A.1.13) (Farquhar et al., 1980), C_a and D (A.2.3). The maximum V_c (V_{cmax}) that drove V_l through the canopy was scaled

from the leaf values by assuming an exponential decrease in V_{cmax} from the top of the canopy to the bottom. This decrease used an extinction coefficient of optimized foliar N distribution, k_N and irradiance, k_b (A.1.3). V_l, g_c, C_i, and D were solved iteratively until energy balance closure was achieved using a set criterion for change in T_c with each iteration.

2.5.2. Autotrophic respiration and changes in phytomass

R_a was the sum of independently calculated values for R_m and R_g (A.4.1). Leaf, sapwood, fine and coarse root R_m were functions of LAI, sapwood volume, and root biomass respectively (A.4.3). Coefficients for each C pool were calculated from R_m measured by Ryan et al. (1997). Leaf, sapwood and root R_m used different Q_{10} temperature functions (A.4.4). R_g was assumed to be 15% of V_c after deducting R_m (A.4.5). A prescribed function based on thermal time was used to allocate growth to new leaves. The remaining V_c, after deducting R_m, R_g, and leaf mass increment, was allocated to stem and root pools by fixed allocation ratios (A.4.6).

2.5.3. Heterotrophic respiration and changes in SOC

R_h was calculated from first-order functions of surface litter C and a single SOC pool in the top two soil layers of CLASS (A.5.1). Litterfall from above-ground plant components contributed to the surface litter pool and litterfall from plant roots contributed to the soil litter pools. Sensitivity of R_h to T_s was given by a Q_{10} coefficient using T_s in the upper 10 cm (Drewitt et al., 2002) (A.5.2). Sensitivity of R_h to θ was not considered for litter, and that for SOC followed Bunnell et al. (1977) and (A.5.3). A prescribed rate of litter C transformation into soil C was used to calculate soil C pool increment (A.5.8 and A.5.10). Other non-gaseous C transfers between different pools were ignored in the version of C-CLASSm used in this study.

2.6. Ecological assimilation of climate and land observations (EALCO)

2.6.1. Background

EALCO was developed at the Canadian Centre for Remote Sensing to study ecosystem–climate interactions by assimilating Earth Observation datasets (both in situ and satellite).

2.6.2. CO_2 and energy exchange

Ecosystem processes of various land cover types were simulated by five main modules including radiation, energy, water, carbon, and nitrogen. The radiation module used multi-canopy layer ray-tracing algorithms based on a gap probability approach (Wang et al., 2002c). Multi-wavelength and separation of direct versus diffuse components for solar radiation were recognized in the model (Wang et al., 2002d). Energy exchange and water uptake were simulated by solving coupled canopy energy and water balance equations (A.6.1, A.6.6), in which T_c and ψ_c were prognostic variables (Wang et al., 2002b).

T_a and D affected CO_2 and energy exchange directly and indirectly through several coupled physiological processes and feedbacks. T_a directly affected V_l through V_r and V_j (A1.2, A.1.8). Temperature indirectly affected g_l through V_l (A.2.1), and thereby affected canopy energy partitioning between H and LE (A.6.1). Values of g_l also controlled C_i, which in turn affected V_l (A.1.5). Relative humidity (RH) affected g_l (Ball, 1988) (A2.1) which directly controlled both C_i and E_c (A.6.1), so that RH affected CO_2 and energy exchange. The interconnected processes by which temperature and humidity affected CO_2 and energy exchange were solved through nested iterations for energy balance closure and C_i.

2.6.3. Autotrophic respiration and changes in phytomass

R_a was the sum of independently calculated values for R_m and R_g (A.4.1). R_m was calculated from plant N (A.4.3) using organ-specific temperature sensitivities (A.4.4). R_g was calculated as a fraction of V_c in excess of R_m (A.4.5), and drove phytomass growth (A.4.6). Litterfall was driven by plant phenological advance (A.4.8).

2.6.4. Heterotrophic respiration and changes in SOC

Litterfall from foliage, stem and roots contributed to soil litter pools (A.4.8). Litter and SOC pools were each divided into three C and N fractions with differing resistance to decomposition, calculated as a first-order function of each pool (A.5.8) with fraction-specific rate coefficients (A.5.9, A.5.10). Also represented in each layer were microbial C and N pools, the latter of which exchanged N with a mineral N pool according to mi-

crobial C:N ratios. Mineral N pools were the source of root N uptake (A.3.2). The decomposition of all litter and SOC pools depended on T_s (A.5.11), ψ_s (A.5.12) and microbial C:N ratio (A.5.8). The fraction of decomposed litter or SOC incorporated into other less active SOC pools was set from pool-specific yield efficiencies, and the remainder was allocated to R_h (A.5.1). Additional N transformations included atmospheric deposition, fertilizer addition, and leaching. Details of soil C and N cycling processes were presented in Wang et al. (2001, 2002a).

2.7. Canadian terrestrial ecosystem model (CTEM)

2.7.1. Background

The Canadian Terrestrial Ecosystem Model (CTEM) is coupled to the Canadian Land Surface Scheme (CLASS) (Verseghy, 2000) to simulate energy, water, and CO_2 fluxes. CTEM is being developed as an operational terrestrial ecosystem model for use in the Canadian Centre for Climate Modelling and Analysis (CCCma) coupled general circulation model.

2.7.2. CO_2 and energy exchange

CO_2 fixation was based on Farquhar et al. (1980) and Collatz et al. (1991, 1992) (A.1.1–A.1.13), and was designed to use both the big- and the two-leaf (sunlit and shaded) scaling techniques (A.2.4). The results presented here were obtained using the big-leaf approach. Canopy stomatal conductance was calculated from CO_2 fixation and D using the Leuning (1995) formulation (A.2.3). *GPP* (A.1), R_a (A.4) and R_h (A.5) sub-modules were described in detail by Arora (2003).

2.7.3. Autotrophic respiration and changes in phytomass

R_a was the sum of independently calculated values for R_m and R_g (A.4.1). T_c and T_s from CLASS were used to estimate R_m from organ-specific coefficients applied to leaf, stem and root (A.4.3, A.4.4). R_g was 0.3 of V_c in excess of R_m (A.4.5). Net CO_2 fixation, after deducting R_a (A.4.1) from V_c (A.1.13), was dynamically allocated between leaves, stem, and roots based on root water, canopy light, and leaf phenology.

2.7.4. Heterotrophic respiration and changes in SOC

Leaf litterfall was generated from leaf turnover driven by a prescribed leaf life span (A.4.8), and by drought and cold stress. Stem and root litterfall were generated by specified turnover times (A.4.8). This litterfall contributed to the soil litter pool which along with SOC generated R_h from first-order respiration coefficients (A.5.1) and from soil temperatures and water contents (A.5.2, A.5.3). R_h drove decomposition of litter and SOC (A.5.8).

3. Modelling experiment

3.1. Experimental sites

3.1.1. Campbell river

The Campbell River (CR) site (49°52′N; 125°20′W; 300 m elevation) in 2000 was a 53-year-old Douglas-fir forest with a sparse understory on a deep humo-ferric podzol. This site is in the drier seasonal rainforest zone found in low and middle elevations of eastern and central Vancouver Island, and is part of the coastal temperate rainforest of the Pacific north-west. Site and soil data are given in Table 1. Urea was applied to this forest at 20 g N m^{-2} in 1994. Eddy covariance techniques used to measure mass and energy fluxes were described in Humphreys et al. (2003). Gap filling techniques to replace rejected eddy-covariance CO_2 fluxes were described in Morgenstern et al. (2004a). Soil water contents through the rooting zone were measured continuously by automated time domain reflectometry (TDR) probes.

3.1.2. Southern Old Jack Pine

The Southern Old Jack Pine (SOJP) site in 2000 was a 71-year-old jack pine forest on an excessively drained Eutrocrept overlying a glacial till south of Narrow Hills Provincial Park, Saskatchewan, Canada (53.9°N 104.7°W) near the southern limit of the boreal forest. Site and soil data are given in Table 2. Eddy covariance techniques used to measure mass and energy exchange were described in Griffis et al. (2003). Gap filling techniques to replace rejected eddy-covariance CO_2 fluxes were described in Barr et al. (2002). Soil water contents through the rooting zone were measured continuously by automated TDR probes.

Table 1
Site and soil characteristics of the Campbell River site

Site characteristics									
Latitude	N49°52.137′								
Longitude	W125°20.120′								
Elevation	300 m								
Mean annual precipitation	1461 mm/y*								
Mean annual temperature	8.3 °C*								
Dominant vegetation	53-year-old Douglas-fir (*Pseudotsuga menziesii*) with 17% red cedar (*Thuja plicata* Donn) and 3% western hemlock (*Tsuga heterophylla* (Raf.) Sarg.)								
Understory vegetation	Sparse, mainly consisting of various mosses, ferns and herbaceous/woody species such as salal, dull oregon grape, vanilla-leaf deerfoot								
Mean basal area (1998)	71 m^2 ha^{-1} (overstory)								
Fertilization	20 g N m^{-2} as urea in 1994								
Horizon	L-H	Ap/Ae	Bf_1	Bf_2/Bf_c					C
Soil characteristics[a]									
Depth to bottom (m)	0.1	0.2	0.3	0.4	0.5	0.6	0.7	0.8	0.9
Bulk density (Mg m^{-3})	0.1	0.90	1.18	1.57	1.50	1.42	1.42	1.58	1.58
Field capacity (m^3 m^{-3})	0.241	0.203	0.203	0.203	0.203	0.203	0.203	0.203	
Wilting point (m^3 m^{-3})	0.117	0.068	0.068	0.068	0.068	0.068	0.068	0.068	
Ksat (mm h^{-1})	36	94	121	133	97	121	107	107	
Sand (g kg^{-1})	–	692	809	880	898	838	883	875	878
Silt (g kg^{-1})	–	227	169	105	93	157	97	98	91
Clay (g kg^{-1})	–	81	23	15	9	6	20	26	31
Coarse fragments (m^3 m^{-3})	0	0.267	0.267	0.353	0.35	0.353	0.356	0.356	0.356
pH	5.2	5.45	5.45	5.92	5.92	5.92	5.0	6.87	5.95
Organic C (g kg^{-1})	81	62.1	28.5	17.5	17.0	18.6	10.0	10.3	8.9
Total N (g Mg^{-1})	1620	640	640	560	560	560	250	200	250
Exch. P (g Mg^{-1})	16	15	15	11	11	11	17	20	20

[a] Keser and St. Pierre, 1973. Soils of Vancouver Island: A compendium. B.C. For Serv. Res. Note 56-Hart soil.

3.2. Model runs

Each model was provided with hourly (CR 1999–2000) or half-hourly (SOJP 1994–2000) meteorological data (shortwave radiation, longwave radiation (C-CLASS and CTEM), air temperature, relative humidity, wind speed and precipitation), and with the site and soil properties in Tables 1 and 2. Model-specific protocols were followed for initialization and spin up, although all models were run for at least 1 year at CR (1999) or 6 years at SOJP (1994–1999) under site conditions before comparison with measured values to reduce sensitivity of model output to model initialization. Model performance was evaluated using parameters (intercepts, slopes) from regressions of modelled on measured fluxes (allowing overestimates or underestimates of measured values to be inferred from intercepts >0 or <0 and from slopes >1 or <1, respectively), and using statistics (coefficients of determination and root mean squares of difference) from regressions of measured on modelled fluxes (allowing differences between modelled and measured fluxes to be expressed in terms of measured values). Model-specific protocols are described in more detail below.

3.2.1. BEPS

The stand ages (Tables 1 and 2) were used to spin up the soil carbon pool with InTEC. Soil water content at the beginning of the modeling period was derived from spin-up model runs using BEPS for 3 years at SOJP and for 7 years at CR. In the spin-up, the initial θ was assumed to be 75% of field capacity as defined in Tables 1 and 2. To reduce the impacts of errors in estimating diurnal heat storage changes in vegetation and soil, the temperatures of the overstory, understory and soil/moss surface and their associated sensible

Table 2
Site and soil characteristics of the Southern Old Jack Pine site

Site characteristics								
Latitude	53°54.976′N							
Longitude	104°41.504′W							
Elevation	579 m							
Mean annual precipitation	390–405 mm							
Mean annual temperature	1.5 °C							
Dominant vegetation	71-year-old Jack Pine *Pinus banksiana*							
Understory vegetation	Reindeer lichen							
Mean basal area (1994)	17 m^2 ha^{-1} (overstory)							
Horizon	LFH	Ae	AB	Bm	C1	C2	Ck	Ck
Soil characteristics[a]								
Depth to bottom (m)	0.04	0.06	0.10	0.38	0.89	1.17	1.69	2.3
Bulk density (Mg m^{-3})	0.24	1.23	1.45	1.48	1.52	1.60	1.60	1.60
Field capacity (m^3 m^{-3})	0.050	0.044	0.029	0.016	0.015	0.017	0.016	
Wilting point (m^3 m^{-3})	0.027	0.026	0.016	0.011	0.009	0.010	0.010	
Ksat (mm h^{-1})	128	124	124	166	173	173	173	
Sand (g kg^{-1})	–	943	934	939	963	975	975	976
Silt (g kg^{-1})	–	29	39	33	19	10	8	10
Clay (g kg^{-1})	–	28	27	28	18	15	17	14
Coarse fragments (m^3 m^{-3})	0	0	0	0	0	0	0	0
pH	4.7	5.3	5.5	5.8	5.8	5.9	6.1	6.2
CEC (cmol$^{(+)}$ kg^{-1})	501	46	40	22	21	16	13	16
Organic C (g kg^{-1})	250.7	9.95	6.43	1.30	0.23	0.17	0.17	0.17
Total N (g Mg^{-1})	4827	430	290	130	120	60	80	70
Total P (g Mg^{-1})	473	150	200	200	190	120	140	190

[a] Anderson, D. 1998. BOREAS TE-01 Soils Data over the SSA Tower Sites in Raster Format, Available online at [http://www-eosdis.ornl.gov/] from the ORNL Distributed Active Archive Center, Oak Ridge National Laboratory, Oak Ridge, TN, USA].

heat fluxes were calculated at 1 min intervals. LAI and clumping index were set to 6.0 and 0.65 at CR, and to 2.4 and 0.7 at SOJP, respectively. The understory LAI was set to 0.5 and 0.8 at CR and SOJP, respectively.

3.2.2. *Ecosys*

Ecosys was initialized at seeding on soil with the properties given in Tables 1 and 2, and with above- and below-ground residue corresponding to that left after logging. *Ecosys* was then run for 54 (CR) or 71 (SOJP) years under repeated 8-year sequences of meteorological data from each site before comparison with measurements. Urea (20 g N m^{-2}) was added to the surface litter layer 6 years before comparison with measurements at CR. Plant parameters used in these runs were those for cool temperate (CR) and boreal (SOJP) conifer functional types which differed only in their temperature sensitivities (A.1.2, A.3.3, A.4.2, A.5.11). Model parameters in *ecosys* are considered to be general in application, and so were not fitted to site-specific data. The rooting zones were considered to be the soil layers described in Tables 1 and 2, the upper of which were subdivided to increase spatial resolution. Two additional soil layers with properties the same as those of the lowest rooted layer and thicknesses of 1–2 m were modelled below the rooting zones. The lower boundary was set so that the water content in the lowest soil layer was maintained at field capacity. These additional layers were intended to enable water fluxes modelled in the rooting zone to be largely independent of assumptions about the lower boundary. *Ecosys* used no additional site data beyond those in Tables 1 and 2.

3.2.3. *C-CLASSa*

C-CLASSa was initialized at seeding on soil with the properties given in Tables 1 and 2, and with above- and below-ground residue corresponding to that left after logging. C-CLASSa was then run for 54 (CR) or 70 (SOJP) years under repeated sequences of meteorological data from each site before comparison with

measurements. Plant parameters used in these runs were those for temperate (CR) and boreal (SOJP) coniferous functional types which differed only in their temperature functions (A.1.2, A.3.3, A.4.2, A.5.11). Model parameters in C-CLASSa are considered to be general in application, and so were not fitted to site-specific data. Rooting depths were set to 0.9 m at CR (Table 1) and 2.3 m at SOJP (Table 2). Root distribution was fixed in the model runs because environmental conditions simulated in the third soil layer could not accurately represent those in the root zone due to the coarse spatial resolution in the model (A.6.7). T_s and θ of the lower soil boundary (depth = 4.1 m) were held constant during the model run. The effects of coarse fragments (Table 1) on soil water retention were simulated at CR. The N deposition rate was set to 7.5×10^{-7} kg N per kg precipitation water and the biological fixation rate was set to 2.8×10^{-9} kg N per kg microbial C per second in the surface layer. Fertilizer N (20 g N m^{-2}) was added to the 10 cm soil layer 6 years before comparison with measurements at CR as indicated in Table 2.

3.2.4. C-CLASSm

Initial C pools (sapwood, coarse and fine root, litter and soil) and soil physical and chemical properties were assigned from site specific measurements given in Tables 1 and 2 according to prescribed soil layer depths (A.6.7). The active root zone was assumed to be the second soil layer in which newly grown roots were allocated to the fine root fraction (A.4.3). Coarse root temperatures were set to T_s of the top soil layer while fine root temperatures were set to T_s of the second soil layer. Rooting depths were set to 0.8 m at CR and 0.6 m at SOJP. The default CLASS root density function (an exponential decrease with depth in A.6.6) was used to set root distribution in the three soil layers. Observed T_s and θ were used to initialize the modelled soil layers at both CR and SOJP. Model simulations were run for 1 year at CR and 6 years at SOJP using observed half-hourly weather data for 2000. Model spin-up was not performed because observed data were used for initialization. Minimum and maximum LAIs prescribed to the model were 6.0 and 6.9 at CR, and 2.0 and 2.0 at SOJP.

3.2.5. EALCO

EALCO was initialized with soil and plant pool sizes estimated from site observations (Tables 1 and 2). Fine root distribution was initialized with 50% in the top 0.35 m and the remainder in the lower 1.15 m. This distribution could change during model runs if differences in root growth rates were simulated among soil layers. The model was run at each site for 2 years with meteorological data from 2000 and results from the second year were compared with measurements. During model runs, simulated LAI was constrained by the maximum observed LAI. No water table was included in these model runs and no gradient in soil matric potential was assumed across the lower soil boundary.

3.2.6. CTEM

At CR, CTEM was initialized with pool sizes derived from site observations and run for 2 years with weather data for 1999 and 2000 with LAI prescribed between 6.0 and 6.9. Model output from the latter year was used in the intercomparison. At SOJP, CTEM was initialized by running for 400 years with weather data from 1997 to 2000 until all live and dead carbon pools had stabilized, after which above-ground biomass was removed to simulate logging. CTEM was then run for another 65 years under repeated sequences of SOJP weather data and a prescribed LAI of 2.0. Output from the last year of this run (corresponding to 2000) was used in the intercomparison.

The rooting depths at both sites were not prescribed in CTEM; rather the model calculated the 99% rooting depth and fraction of roots in each soil layer using simulated or specified root biomasses based on a variable rooting depth parameterization described in Arora and Boer (2003). Soil physical properties at both sites were estimated from Tables 1 and 2, including fractions of sand and clay for the three soil layers used in CLASS.

4. Results

4.1. Diurnal energy and CO_2 exchange under changing temperature-measurement

4.1.1. Campbell river

The passage of a warm front during late June 2000 provided an opportunity to test model responses to transient warming at CR. Maximum/minimum daily temperatures rose from 17/10 to 28/19 °C under clear skies between 21 and 26 June 2000 (DOY 173–178) and then declined sharply under cloudy skies after 28 June (DOY 180) (Fig. 1a). During this period, θ measured by au-

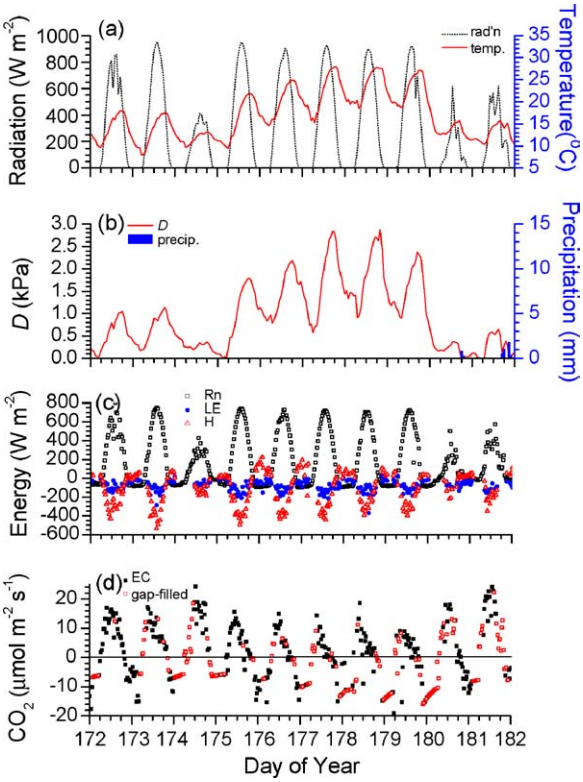

Fig. 1. (a) Radiation and temperature, (b) vapor pressure deficit (D) and precipitation, (c) energy fluxes, and (d) CO_2 fluxes (positive fluxes downwards) recorded or gap-filled at Campbell River during 21–30 June 2000 (DOY 173–182). Downward fluxes were assigned positive values, and upward fluxes negative values.

tomated TDR probes from 0.0 to 0.6 m depth declined from 0.23 to 0.21 $m^3\ m^{-3}$, close to field capacity for the soil at CR (Table 1). Daily D rose during warming from 1 kPa to almost 3 kPa and then declined during cooling (Fig. 1b). Daytime LE measured by eddy covariance rose from 150 $W\ m^{-2}$ before warming ($D \sim 1$ kPa) to 200 $W\ m^{-2}$ at the onset of warming on DOY 176 ($D \sim 1.75$ kPa), but then declined to <200 $W\ m^{-2}$ with further warming on DOY 177–179 ($D \sim 2.75$ kPa), and remained stable during cooling on DOY 181–182 ($D \sim 0.5$ kPa) (Fig. 1c). Peak CO_2 influxes declined from 20 to 15 $\mu mol\ m^{-2}\ s^{-1}$ during warming on DOY 176–180 and then rose to >20 $\mu mol\ m^{-2}\ s^{-1}$ during subsequent cooling on DOY 182 (Fig. 1d). Midafternoon declines in CO_2 influxes began earlier and were more rapid under higher D (DOY 177–180) than under lower (DOY 175, 182). Peak CO_2 effluxes rose from 6 to >12 $\mu mol\ m^{-2}\ s^{-1}$ during warming on DOY 176–180, although wind speeds caused many of the measured nighttime effluxes to be rejected and replaced by gap-filled values.

4.1.2. *Southern Old Jack Pine*

A warm front during mid-July 2000 provided an opportunity to test model responses to transient warming at SOJP. Maximum/minimum daily temperatures rose from 20/13 °C during 6–11 July 2000 (DOY 188–193) to 30/18 °C on 14 July 2000 (DOY 196) and returned to 22/13 °C on 15 July 2000 (DOY 197) (Fig. 2a). During this period, θ measured by automated TDR probes from 0.0 to 0.6 m depth varied between 0.08 and 0.10 $m^3\ m^{-3}$, well above the very low field capacity for the soil at SOJP (Table 2). Daily D rose from <1 to 3 kPa during warming until DOY 196 and then

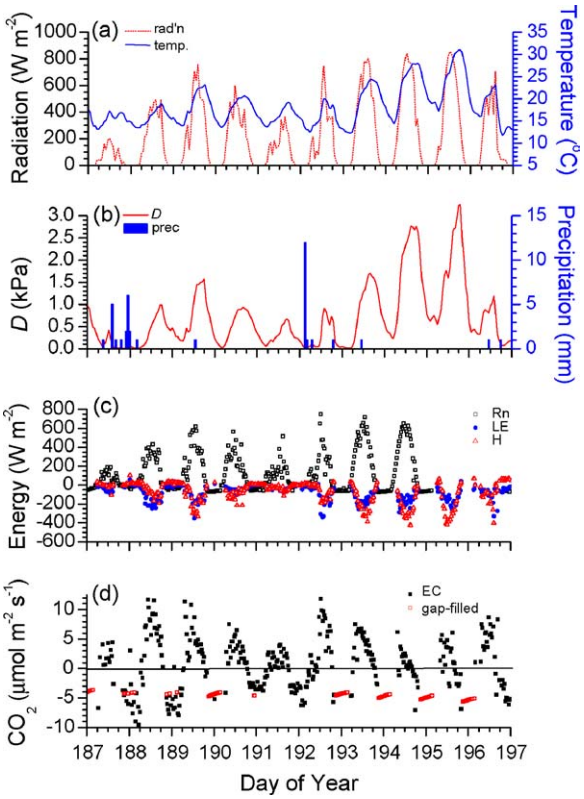

Fig. 2. (a) Radiation and temperature, (b) vapor pressure deficit (D) and precipitation, (c) energy fluxes, and (d) CO_2 fluxes (positive fluxes downwards) recorded or gap-filled at Southern Old Jack Pine during 6–15 July 2000 (DOY 188–197). Downward fluxes were assigned positive values, and upward fluxes negative values.

returned to <1 kPa during DOY 197 (Fig. 2b). Daytime *LE* measured by eddy covariance reached 200 W m^{-2} under intermediate radiation and *D* during DOY 189 and 190, but did not rise further under higher radiation and *D* during DOY 194 through 196 (Fig. 2c). Both influxes and effluxes of CO_2 measured at SOJP (Fig. 2d) were ~1/2 those measured at CR (Fig. 1d). Peak CO_2 influxes declined from 10 to 5 μmol m^{-2} s^{-1} and midday declines in CO_2 influxes began earlier as warming progressed during DOY 194–196 (Fig. 2d). Most nighttime CO_2 effluxes measured during this period were rejected due to low wind speeds, and were replaced by effluxes calculated from gap-filling methods.

4.2. Diurnal energy exchange under changing temperature-modelling

4.2.1. BEPS

LE effluxes modelled at CR rose above 200 W m^{-2} when *D* rose from 1.0 kPa (DOY 173) to 1.75 kPa (DOY 176) but rose little with further rises in *D* from 1.75 kPa (DOY 177) to 3.0 kPa (DOY 180) (Fig. 3a), indicating that effects of *D* on *LE* (A.6.1) were offset by those on g_l (A.2.1). *LE* effluxes were larger than those measured and *H* effluxes were smaller, especially under higher *D* (DOY 179–180), suggesting that *D* effects on g_l were underestimated by the empirical equation developed at CR (Humphreys et al., 2003) (A.2.1). *LE* effluxes modelled at SOJP remained <200 W m^{-2} when VPD rose above 1.5 kPa (DOY 194–196) (Fig. 4a) so that *H* effluxes were not underestimated, indicating a strong constraint by *D* on g_l in the empirical equation developed for boreal forests (Dang et al., 1997) (A.2.1). Modelled *LE* effluxes were smaller than those measured under higher *D*, indicating some errors in calculating $f(\psi_s)$ in A.2.1 for this very sandy soil (Table 2).

4.2.2. Ecosys

Soils at CR and especially SOJP had low organic C and high C:N ratios (Tables 1 and 2) that constrained N uptake (A.3.2), causing low leaf non-structural N:C ratios that limited V_r (A.1.3, A.1.9), causing low g_{lmax} (A.2.1) and hence low *LE* versus *H* (A.6.1) (Figs. 3b and 4b). The onset of higher temperature and *D* during DOY 176–178 at CR and DOY 193–194 at SOJP raised *LE* effluxes to >200 W m^{-2} (A.6.1), forcing lower ψ_c to maintain root water uptake and canopy hydration (A.6.6). Values of ψ_c in *ecosys* were more

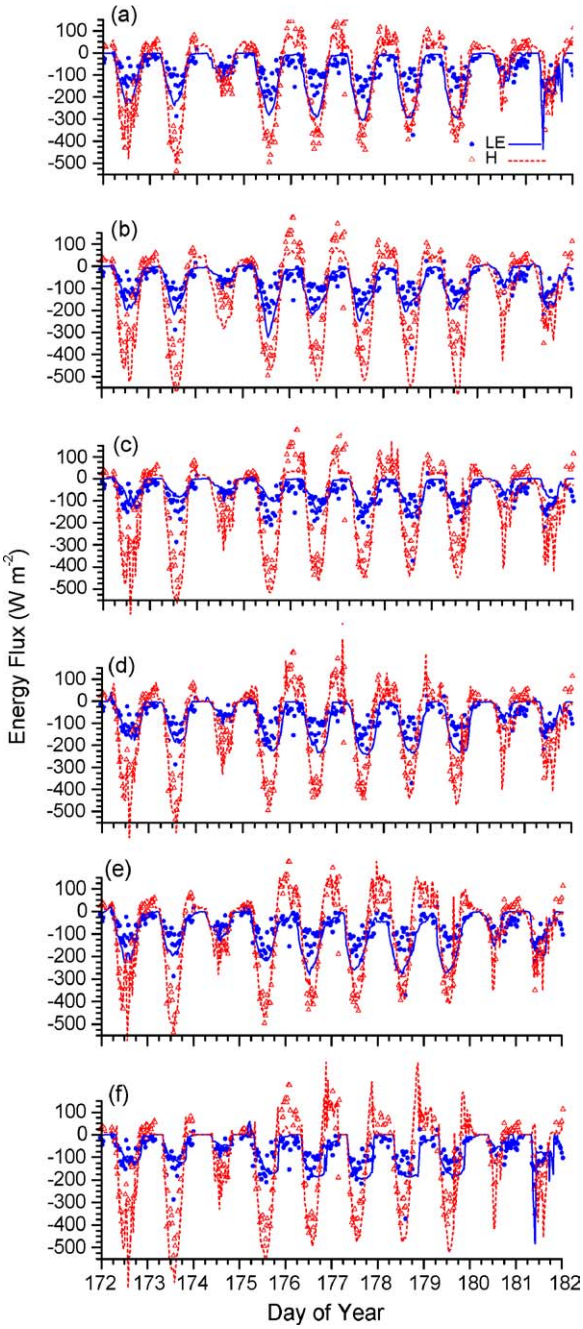

Fig. 3. Latent (LE) and sensible (H) heat fluxes measured by eddy covariance (symbols) and modelled (lines) by (a) BEPS, (b) *ecosys*, (c) C-CLASSa, (d) C-CLASSm, (e) **EALCO** and (f) **CTEM** at Campbell River during 21–30 June 2000 (DOY 173–182). Downward fluxes were assigned positive values, and upward fluxes negative values (i.e. reverse order of *EALCO* and *CTEM*).

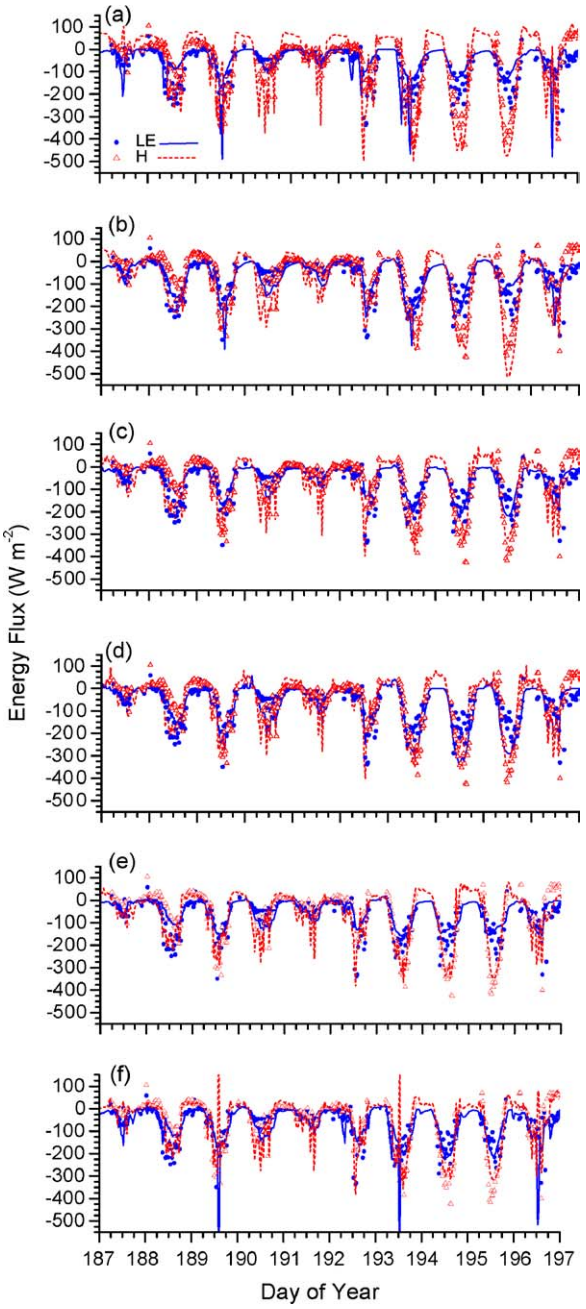

Fig. 4. Latent (LE) and sensible (H) heat fluxes measured by eddy covariance (symbols) and modelled (lines) by (a) BEPS, (b) *ecosys*, (c) C-CLASSa, (d) C-CLASSm, (e) **EALCO** and (f) **CTEM** at Southern Old Jack Pine during 6–15 July 2000 (DOY 188–197). Downward fluxes were assigned positive values, and upward fluxes negative values (i.e.reverse order of *EALCO* and *CTEM*).

sensitive to root water uptake in conifers than in other plant functional types because of the larger value for root axial resistivity used to calculate root axial resistance Ω_a. Large Ω_a delayed rehydration and hence recovery of ψ_c and *LE* when *D* declined during later afternoons and evenings. With further warming during DOY 179–180 at CR and DOY 195–196 at SOJP, lower ψ_c forced lower ψ_T that reduced g_c (A.2.2) and hence reduced canopy *LE* to <200 W m^{-2} (A.6.1). Values of θ and hence ψ_s were sensitive to soil drying at CR because a large fraction of soil was excluded from water retention and transfer by coarse fragments (Table 1), and at SOJP because of extremely low water holding capacity (Table 2). The combined result of these algorithms was a small increase in *LE* with the onset of warming and then decreases with further warming, consistent with measured fluxes at both sites.

4.2.3. C-CLASSa

High soil C:N ratios (Tables 1 and 2) caused low N uptake (A.3.2) and hence low leaf structural and nonstructural N:C ratios that constrained V_l (A.1.3, A.1.9), g_l (A.2.1) and hence *LE* versus *H* (A.6.1). Modelled *LE* remained <200 W m^{-2} at CR, below that measured when $D < 1.5$ kPa (DOY 173–176, 181–182), but close to that measured when $D > 1.5$ kPa (DOY 177–180) (Fig. 3c). Modelled *LE* at SOJP rose to 200 W m^{-2} when *D* rose to 1.5 kPa (DOY 194) (Fig. 4c), but further rises in modelled *LE* when $D > 1.5$ kPa at CR and SOJP were constrained by the effect of RH on g_l (A.2.1) and thereby on E_c (A.6.1). Model underestimates of *LE* at SOJP on DOY 189 and 193 following rainfall events (Fig. 4c) were likely caused by r_a calculated for canopy and soil surface evaporation (A.6.2–A.6.4).

4.2.4. C-CLASSm

Low V_l caused low g_l which in turn caused large *H* versus *LE* to be modelled by C-CLASSm at CR (Fig. 3d) and SOJP (Fig. 4d). Midday *LE* effluxes reached 150 W m^{-2} during cool days (DOY 172–173) when low *D* (<1.5 kPa) caused higher g_l (A.2.1) and hence g_c (A.2.3). Midday *LE* reached 200 W m^{-2} when *D* rose above 1.5 kPa (DOY 176), although further increases in *LE* when $D > 2.0$ kPa were constrained by the effect of *D* on g_l (A.2.1). Low *D* caused low vapor concentration gradients and hence low *LE* to be modelled during DOY 181–182 (A.6.1). *LE* effluxes modelled at SOJP reached 300 W m^{-2} when

D rose to 2.5 kPa during warming on DOY 193–195, and then declined slightly when D rose further to 3 kPa on DOY 196. Rises in LE modelled during warming at both sites were larger than those measured, indicating that the constraint of D on g_l may have been underestimated, especially at SOJP where a larger value of D_0 was used (A.2.1).

4.2.5. EALCO

Modelled LE effluxes were close to those measured at CR when $D < 1.5$ kPa, although they were larger when $D > 1.5$ kPa on DOY 177–180 (Fig. 3e). This overestimation may indicate that RH effects on g_l in the model (A.2.1) were underestimated. Some of this overestimation of LE may be attributed to the large value for the slope parameter used to calculate g_l (A.2.1). Overestimation of LE under high D was not apparent at SOJP where rising D lowered LE effluxes modelled on DOY 194–196 (Fig. 4e).

4.2.6. CTEM

Modelled LE rose with D until D reached 1.5 kPa on DOY 176, after which further rises were constrained by effects of D on g_c (A.2.3) (Fig. 3f). However LE effluxes modelled under higher D on DOY 177–180 remained larger than those measured, indicating that the modelled effect of D on g_c (A.2.3) at CR may have been underestimated. LE effluxes modelled under high D at CR maintained maximum diurnal values of 150 W m^{-2} through early afternoon and evening, in contrast to measured effluxes which reached maximum values by late morning and then declined after midday. These larger LE effluxes caused brief H influxes to be modelled near dusk that were not apparent in the measurements. LE effluxes modelled at SOJP declined more rapidly after midday than did those at CR (Fig. 4f), although CTEM used a common value for D_0 at both sites (A.2.3). Some instability in modelled energy balances was found to be caused by the aerodynamic resistance formulation in CLASS from which the energy exchange algorithms in CTEM were taken.

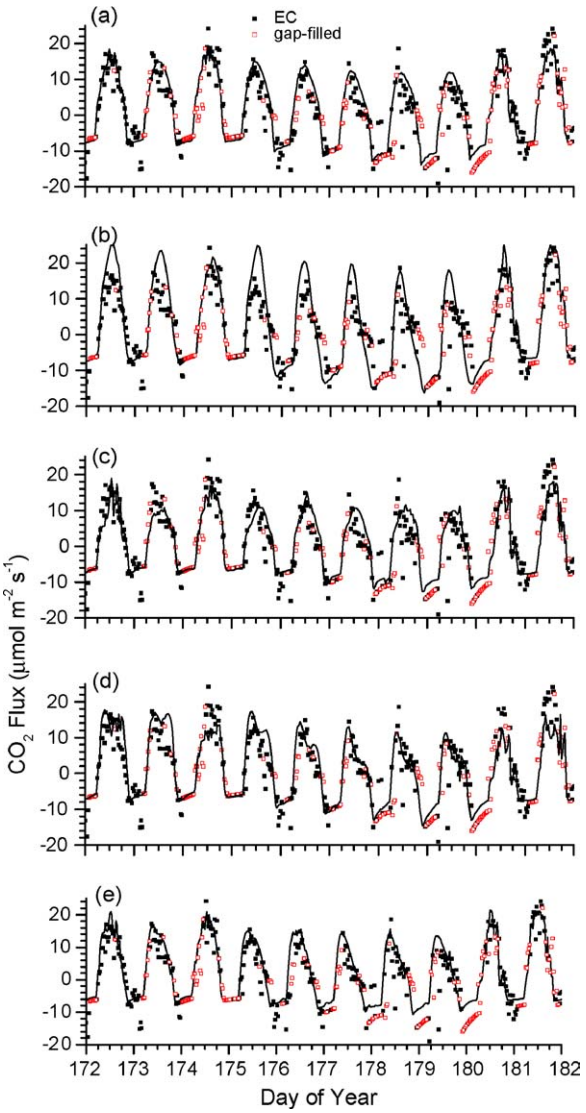

Fig. 5. CO_2 exchange measured by eddy covariance (symbols) and modelled (lines) by (a) BEPS, (b) *ecosys*, (c) C-CLASSa, (d) C-CLASSm, and (e) EALCO at Campbell River during 21–30 June 2000 (DOY 173–182). Downward fluxes were assigned positive values, and upward fluxes negative values.

4.3. Diurnal CO_2 exchange under changing temperature-modelling

4.3.1. BEPS

Contrasting effects of T_c on V_c (A.1.2, A.1.8) versus those of T_c and T_s on R_a (A.4.3, A.4.4) and R_h (A.5.11) enabled BEPS to model declining influxes and rising effluxes of CO_2 during warming at CR (DOY 177–180) (Fig. 5a) and SOJP (DOY 194–196) (Fig. 6a). Earlier midday declines in CO_2 influxes were clearly modelled at SOJP where ψ constraints on g_l were larger (A.2.2), but not at CR where ψ was more favorable. Nighttime

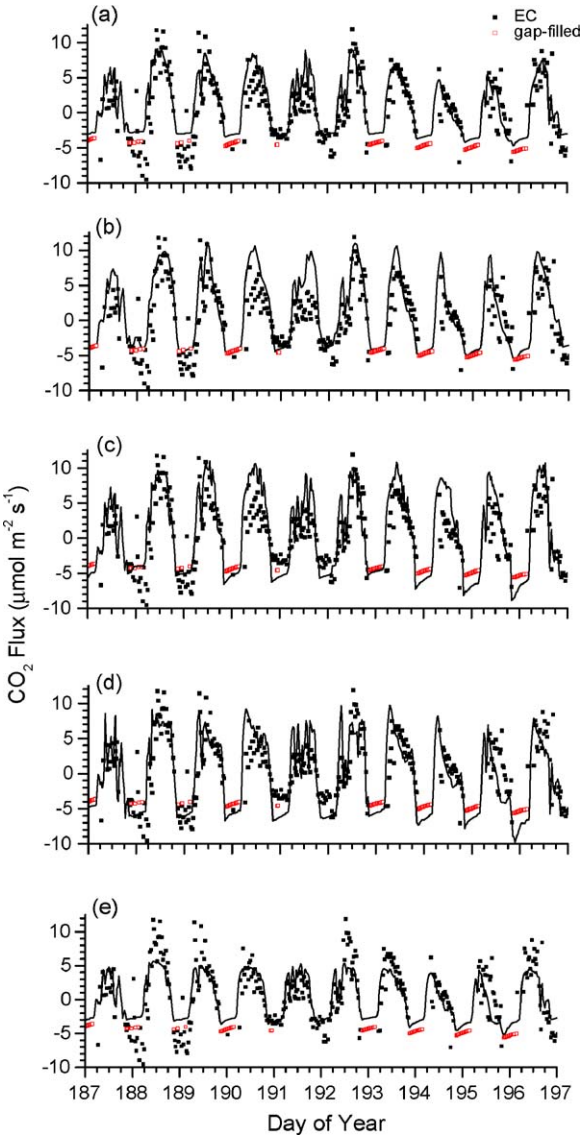

Fig. 6. CO_2 exchange measured by eddy covariance (symbols) and modelled (lines) by (a) BEPS, (b) *ecosys*, (c) C-CLASSa, (d) C-CLASSm, and (e) EALCO at Southern Old Jack Pine during 6–15 July 2000 (DOY 188–197). Downward fluxes were assigned positive values, and upward fluxes negative values.

CO_2 effluxes in the model were smaller than those measured or gap-filled during warming at CR (Fig. 3a) and SOJP (Fig. 7a), due to comparatively low rate coefficients for root R_m (A.4.3) and for soil C decomposition (A.5.9).

4.3.2. Ecosys

CO_2 fluxes modelled at SOJP were reduced to less than one-half those at CR (Fig. 6b versus Fig. 5b) by slower soil mineralization (A.4.2) and root uptake (A.3.3) from colder soils. CO_2 fluxes modelled at SOJP were also reduced by lower LAI (2.2 at SOJP versus 8.5 at CR) caused by reduced leaf growth from lower leaf N concentrations and more frequent water stress on soil with a lower water holding capacity (Table 2 versus Table 1). V_c and above-ground R_a were both driven by T_c (A.1.2, A.4.2), and rose sharply with the onset of warming. Below-ground R_a and R_h, driven by T_s (A.4.2, A.5.2) which was less sensitive than T_c to short-term warming, rose less sharply. With further temperature rises, the effect of warming on V_c was overridden by the combined effects (A.1.13) of stomatal (A.2.2) and non-stomatal (A.1.4) constraints imposed by declining ψ_c (A.6.6). Constrained V_c and rising $R_a + R_h$ caused earlier midday declines in CO_2 influxes during warming on DOY 177–179 at CR (Fig. 5b) and DOY 194–196 at SOJP (Fig. 6b). Daytime CO_2 influxes returned to higher values with no midday declines when ψ_c constraints on V_c were alleviated by lower D during cooling on DOY 181–182 at CR and DOY 197 at SOJP. Rises in $R_a + R_h$ caused nighttime CO_2 effluxes to exceed 10 $\mu mol\ m^{-2}\ s^{-1}$ during warming at CR (Fig. 5b) although CO_2 effluxes rose less with warming at SOJP (Fig. 6b).

4.3.3. C-CLASSa

Contrasting effects of T_c on V_c (A.1.2, A.1.8) versus those of T_c and T_s on R_a (A.4.3, A.4.4) and R_h (A.5.11) enabled C-CLASSa to simulate smaller daytime influxes and larger nighttime effluxes of CO_2 during warm days (DOY 177–179) than during cool days (DOY 173–175, 181–182) at CR (Fig. 5c). Large CO_2 influxes of ~20 $\mu mol\ m^{-2}\ s^{-1}$ measured at CR under low radiation, temperature and D during DOY 175 and 182 were underestimated, causing lower g_l (A.2.1) and hence LE (Fig. 3c) in the model. Lower soil C and N contents (Table 2) and lower T_s modelled at SOJP versus CR caused slower N mineralization (A.5.11) and uptake (A.3.3). This caused greater N limitation to V_r and V_j (A.1.3, A.1.9), so that CO_2 influxes and effluxes modelled at SOJP were smaller than those at CR (Fig. 6c versus 5c). Both influxes and effluxes modelled at SOJP were larger than those measured or es-

timated by gap-filling (Fig. 6c). CO_2 influxes modelled at SOJP did not rise during warming on DOY 194–196 because of the lower optimum temperature for plant and soil processes used at this site (A.1.2). However earlier midafternoon declines in CO_2 influxes measured under higher temperature and D were not clearly simulated at either site (Figs. 5c and 6c), indicating that the RH term used to calculate g_l (A.2.1) may not be sensitive enough to D at higher temperatures. This indication was corroborated by the tendency of modelled LE influxes to rise under higher D (Figs. 3c and 4c).

4.3.4. C-CLASSm

CO_2 influxes simulated at both CR and SOJP were larger during cool days (DOY 173–174, 182 at CR, DOY 189–191, 197 at SOJP) than during warm days (DOY 176–180 at CR, DOY 194–196 at SOJP) (Figs. 5d and 6d). CO_2 influxes were very sensitive to D. Earlier midday declines in these influxes were simulated on warm days which was consistent with measurements, but also on some cool days which was not consistent with measurements (e.g. DOY 182 at CR, DOY 197 at SOJP). These declines could have been caused by low θ when used in the function f_w (A.1.4) to calculate g_l (A.2.1). However LE effluxes appeared to be less sensitive to D than were CO_2 influxes (Figs. 3d and 4d). This function would require soil-specific parameterization, especially for the very sandy soils underlying most boreal forests (e.g. Table 2).

Higher T_a and T_s increased both R_a (A.4.4) and especially R_h (A.5.2), causing nighttime CO_2 effluxes to rise at both sites. The larger effluxes simulated by C-CLASSm in comparison to those by the other models may be attributed to its larger rate constant (A.5.1) and temperature sensitivity (A.5.2) for R_h of SOC. Rates of net CO_2 exchange simulated in C-CLASSm at SOJP (Fig. 6d) were lower than those at CR (Fig. 5d), although key photosynthetic parameters, including $V_{rmax(0)}$, were the same at both sites (A.1.1). These lower rates were attributed to the lower LAI prescribed for SOJP (2–2.6 $m^2\,m^{-2}$) versus CR (6–6.9 $m^2\,m^{-2}$) used to calculate canopy V_{rmax} (A.1.1), J_{max} (A.1.6), and leaf R_m (A.4.3). As did most other models, C-CLASSm underestimated large CO_2 influxes measured under low radiation, temperature and D on DOY 175, 181 and 182 at CR, and on DOY 189, 190 and 197 at SOJP.

4.3.5. EALCO

Peak CO_2 influxes modelled at CR declined from 20 $\mu mol\,m^{-2}\,s^{-1}$ under lower temperature and D (DOY 175, 181–182) to 15 $\mu mol\,m^{-2}\,s^{-1}$ under higher temperature and D (DOY 177–180) (Fig. 5e) when lower RH raised E_c (A.6.1), thereby reducing ψ_c (A.6.4), C_i, and hence V_r (A.1.4). CO_2 influxes were further reduced under higher T_a by larger R_a (A.4.4) and R_h (A.5.11). However CO_2 effluxes in the model rose less with warming than did those estimated from eddy covariance measurements at CR, suggesting that temperature effects on R_m and/or R_h may be underestimated. Both influxes and effluxes of CO_2 modelled at SOJP were frequently smaller than those measured or gap-filled (Fig. 6e), causing a corresponding underestimation of LE (Fig. 4e) in spite of the large slope used to calculate g_l (A.2.1). The smaller effluxes may be partly attributed to the small rate constant used for R_h from SOC (A.5.1) when SOC was small (Table 2). Midafternoon declines in CO_2 influxes at CR and SOJP when $D > 2.5$ kPa were modelled from ψ_c effects on V_r (A.1.4) and from D effects on g_l (A.2.1).

4.3.6. CTEM

Diurnal R_a and R_h were not simulated by CTEM so that short-term weather effects on modelled CO_2 fluxes could not be evaluated.

4.4. Daily net ecosystem productivity under changing temperature-measurement

Higher T_a caused declines in afternoon CO_2 influxes and rises in nighttime CO_2 effluxes at both CR (Fig. 1d) and SOJP (Fig. 2d). These changes in CO_2 fluxes caused changes in daily NEP at both sites during the major warming events in the summer of 2000 (Figs. 7 and 8). CR changed from a sink of 2–5 $g\,C\,m^{-2}\,d^{-1}$ under lower T_a (DOY 170–175, DOY 180–195, DOY 205–215) to a source of 2–5 $g\,C\,m^{-2}\,d^{-1}$ under higher T_a (DOY 177–180, DOY 200–204, DOY 216–219) (Fig. 7). Similarly, SOJP changed from a small sink of 0–1 $g\,C\,m^{-2}\,d^{-1}$ under lower T_a (DOY 170–178, DOY 183–193, DOY 198–203) to a source of 1–3 $g\,C\,m^{-2}\,d^{-1}$ under higher

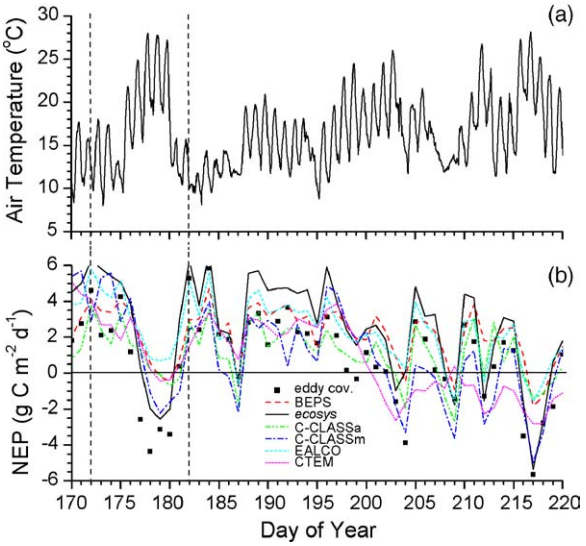

Fig. 7. (a) Hourly air temperature and (b) daily net ecosystem productivity calculated from gap-filled eddy covariance measurements (symbols) and modelled (lines) at Campbell River during summer 2000. Vertical lines indicate period shown in Figs. 1, 3 and 5.

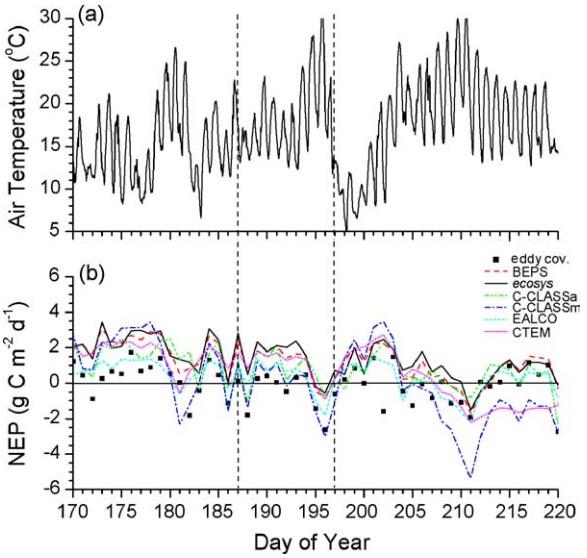

Fig. 8. (a) Hourly air temperature and (b) daily net ecosystem productivity calculated from gap-filled eddy covariance measurements (symbols) and modelled (lines) at Southern Old Jack Pine during summer 2000. Vertical lines indicate period shown in Figs. 2, 4 and 6.

T_a (DOY 179–182, DOY 194–197, DOY 208–211) (Fig. 8). All models captured the direction of change in daily *NEP* during warming, although the magnitude of change varied among models as indicated from regressions of modelled versus measured *NEP* during these periods (Table 3).

4.5. Daily net ecosystem productivity under changing temperature-modelling

4.5.1. BEPS

BEPS accurately modelled sinks under lower T_a at both CR (Fig. 7) and SOJP (Fig. 8). However BEPS modelled smaller sources under higher T_a than were

Table 3
Statistics from regressions of simulated on measured (b,a), and measured on simulated (R^2, RMSD), daily net ecosystem productivity (*NEP*) during major warming events in summer 2000 at (a) Campbell River (CR) and (b) Southern Old Jack Pine (SOJP)

	BEPS	*Ecosys*	C-CLASSa	C-CLASSm	EALCO	CTEM
(a) CR						
NEP ($n = 50$)						
b[a]	0.52	1.04	0.47	0.75	0.61	0.52
a (g m^{-2} d^{-1})	1.72	1.63	0.70	0.24	1.84	0.38
R^2	0.73	0.87	0.62	0.55	0.75	0.42
RMSD (g m^{-2} d^{-1})	1.36	0.95	1.60	1.74	1.30	1.98
(b) SOJP						
NEP ($n = 50$)						
b	0.76	0.68	0.68	1.20	0.57	0.47
a (g m^{-2} d^{-1})	1.30	1.41	0.88	0.13	0.40	0.68
R^2	0.52	0.43	0.42	0.36	0.46	0.12
RMSD (g m^{-2} d^{-1})	0.74	0.81	0.81	0.86	0.79	1.01

[a] $Y = a + bX$ from regression of simulated Y on measured X, R^2 and RMSD = coefficient of determination and root mean square for difference from regression of measured Y on simulated X.

measured at both sites (e.g. DOY 177–180 and DOY 216–219 at CR) because earlier midday declines in CO_2 influxes under higher D were not simulated and CO_2 effluxes were slightly smaller than those measured (Figs. 5a and 6a). Consequently the magnitude of change between sink and source was only partially captured with a bias towards sinks ($b < 1$, $a > 0$ in Table 3).

4.5.2. Ecosys

Larger modelled versus measured CO_2 influxes (Figs. 5b and 6b) caused *ecosys* to give larger sinks and smaller sources than measured at both sites ($a > 0$ in Table 3a and b). However earlier midday declines in CO_2 influxes modelled under higher D allowed *ecosys* to capture the full extent of change in *NEP* with warming at CR (Fig. 7; $b \rightarrow 1$ in Table 3a), but only partially at SOJP (Fig. 8; $b < 1$ in Table 3b).

4.5.3. C-CLASSa

C-CLASSa accurately modelled sinks under lower T_a, but gave smaller sources than were measured under higher T_a at CR (Fig. 7) and SOJP (Fig. 8) ($a > 0$ in Table 3a and b). The magnitude of change in *NEP* with warming was thereby underestimated ($b < 1$ in Table 3a and b), even though CO_2 effluxes were not underestimated, because earlier midday declines in CO_2 influxes under higher D were not modelled (Figs. 5c and 6c).

4.5.4. C-CLASSm

C-CLASSm gave large declines in midday CO_2 influxes under higher D (Figs. 5d and 6d), due to the sensitivity of V_l to D (A.2.1, A.1.13). C-CLASSm also gave large rises in CO_2 effluxes during warming due to the sensitivity of R_h to T_s in A.5.2. These sensitivities enabled accurate estimation of sources during warmer periods at both CR (DOY 177–180 and DOY 216–219 in Fig. 7; $b \rightarrow 1$ in Table 3a) and SOJP (DOY 179–182 and DOY 194–197 in Fig. 8), but also overestimation of late summer sources at SOJP (DOY 208–211 in Fig. 8; $b > 1$ in Table 3b). These sensitivities of *NEP* to warming in the model caused bias to be low at both sites ($a \rightarrow 0$ in Table 3a and b).

4.5.5. EALCO

Low CO_2 effluxes modelled by EALCO at both sites (Figs. 5e and 6e from low rate constant for R_h of SOC in A.5.1) caused CR in the model to remain a sink during warming on DOY 177–180, and to be a smaller source than estimated from measurements during other warming events (e.g. DOY 216–219) (Fig. 7; $b < 1$, $a > 0$ in Table 3a). Low CO_2 effluxes modelled by EALCO at SOJP were offset by low CO_2 influxes (Fig. 6e) so that changes from sinks to sources modelled during warming events (e.g. DOY 194–196 and DOY 208–211 in Fig. 8) were smaller than those measured, but were not greatly biased ($b < 1$, $a \rightarrow 0$ in Table 3b).

4.5.6. CTEM

CTEM underestimated sources during warming events before DOY 200 at CR (Fig. 7) and SOJP (Fig. 8) but underestimated sinks afterwards at both sites. Smaller changes with T_a in modelled versus measured *NEP* reduced agreement with measured values (lower slope (b), coefficient of determination (R^2), and higher root mean squares for differences (RMSD) than other models in Table 3). Lower variability of modelled versus measured *NEP* could have been caused by simulating R_a and R_h at a daily time step so that diurnal variation in CO_2 effluxes was not modelled. Also, CTEM used generalized, and not site-specific, values for Q_{10} of both R_a (A.4.4) and R_h (A.5.2).

4.6. Annual energy and CO_2 fluxes

Comparison with annual energy and CO_2 fluxes (Table 4) provided a general test of model response to diverse environmental signals at an annual time scale, extending the previous, more constrained test of model response to warming at a seasonal time scale (Table 3). Measurements of annual R_n were closely simulated by all models ($a \rightarrow 0$, $b \rightarrow 1$ in Table 4) because measured shortwave radiation was provided as a model input. Measurements of *LE* and *H* used in model testing were not corrected for incomplete closure of the energy balance (yearly average of 0.88 at CR and 0.85 at SOJP). Slopes from regressions of modelled on measured *LE* at CR indicated comparable performances by all models ($b \rightarrow 1$) except C-CLASSa, where *LE* was underestimated ($b = 0.52$ in Table 4a) as seen in Fig. 3c. RMSD between measured and modelled *LE* indicated that the models could not explain $\sim$30 W m^{-2} of the measured fluxes, with no significant differences among models. Most models except *ecosys* and C-CLASSm underestimated *LE* at SOJP ($b < 0.8$ in Table 4b) as seen in Fig. 4. Values of R^2 and RMSD for *LE* at SOJP were comparable to those at CR for all models except BEPS

Table 4
Statistics from regressions of simulated on measured (b,a), and measured on simulated (R^2, RMSD), hourly averaged net radiation (Rn), latent heat (LE), sensible heat (H) and net CO_2 exchange (CO_2) during 2000 at (a) Campbell River (CR) and (b) Southern Old Jack Pine (SOJP)

	BEPS	*Ecosys*	C-CLASSa	C-CLASSm	EALCO	CTEM
(a) CR						
Rn (n = 8776)						
b[a]	0.95	1.02	0.90	0.97	0.95	1.01
a (W m^{-2})	−20	5	12	2	1	−9
R^2	0.95	0.95	0.98	0.98	0.94	0.96
RMSD (W m^{-2})	41	41	24	24	43	35
LE (n = 3571)						
b	1.16	1.05	0.52	0.91	1.02	0.98
a (W m^{-2})	12	12	6	12	9	11
R^2	0.65	0.62	0.56	0.57	0.58	0.53
RMSD (W m^{-2})	29	30	32	32	31	33
H (n = 3738)						
b	1.07	1.20	1.08	1.08	1.00	1.08
a (W m^{-2})	−20	−66	−76	−60	−51	−39
R^2	0.85	0.87	0.89	0.85	0.80	0.80
RMSD (W m^{-2})	50	46	44	50	58	57
CO_2 (n = 3740)						
b	0.89	1.04	0.76	0.85	0.83	
a (μmol m^{-2} s^{-1})	0.8	0.6	0.4	0.7	0.8	
R^2	0.84	0.79	0.81	0.79	0.84	
RMSD (μmol m^{-2} s^{-1})	3.4	3.8	3.5	3.8	3.4	
(b) SOJP						
Rn (n = 7838)						
b	0.95	0.98	0.91	1.00	0.93	0.94
a (W m^{-2})	−33	11	2	2	−8	0
R^2	0.84	0.96	0.99	1.00	0.94	0.99
RMSD (W m^{-2})	64	31	15	7	40	18
LE (n = 4476)						
b	0.47	0.85	0.68	1.03	0.63	0.75
a (W m^{-2})	−14	−6	−6	−6	−9	−7
R^2	0.32	0.68	0.63	0.65	0.62	0.51
RMSD (W m^{-2})	40	27	29	29	30	34
H (n = 4532)						
b	1.08	1.07	0.86	0.94	0.80	0.80
a (W m^{-2})	29	−17	−20	−11	−9	−13
R^2	0.62	0.79	0.79	0.79	0.66	0.75
RMSD (W m^{-2})	70	52	52	52	66	56
CO_2 (n = 4361)						
b	0.77	0.79	0.91	1.02	0.56	
a (μmol m^{-2} s^{-1})	0.2	0.1	0.3	0.2	0.2	
R^2	0.63	0.61	0.61	0.64	0.58	
RMSD (μmol m^{-2} s^{-1})	1.8	1.8	1.8	1.8	1.9	

[a] $Y = a + bX$ from regression of simulated Y on measured X, R^2 = coefficient of determination from regression of Y on X, RMSD = root mean square for error from regression of measured Y on simulated X.

and CTEM which experienced occasional convergence problems at SOJP (Fig. 4a and f). Regression statistics for *LE* at both sites were adversely affected by large *LE* effluxes measured but not modelled during some afternoons (e.g. DOY 174, 177 and 179 in Fig. 3 and DOY 233 and 239 in Fig. 4). Slopes from regressions of modelled on measured *H* at both CR and SOJP were slightly larger than those on *LE*, indicating that energy dissipation was partitioned somewhat more to *H* than to *LE* in the models than in the eddy covariance measurements.

Slopes from regressions of modelled on measured CO_2 fluxes at CR were similar ($b > 0.8$) for all models except C-CLASSa, the slope of which was smaller (Table 4a) as was the that for summer daily *NEP* (Table 3a). Slopes at SOJP were largest for C-CLASSa and C-CLASSm ($b \rightarrow 1$), lower for BEPS and *ecosys* ($b \sim 0.8$), and lowest for EALCO ($b < 0.6$) (Table 4b; also see Fig. 6e). These slopes followed the same order as those for summer daily *NEP*, except for C-CLASSa (Table 3b). Model theory would suggest that if the interdependence between V_l and g_l were correctly parameterized (A.2.1), then *b* values for regressions of modelled on measured CO_2 fluxes should have been similar to those for *LE*. However C-CLASSa and EALCO modelled larger and smaller *b* respectively for CO_2 than for *LE* at both sites, indicating that their parameters in A.2.1 may need to be reviewed. The large *m* used in EALCO to calculate g_l (A.2.1) likely compensated for low V_l (Figs. 5e and 6e; Table 4b) in modeling *LE* (Figs. 3e and 4e). Values of RMSD between measured and modelled CO_2 fluxes indicated that the models could not explain $\sim$3.5 μmol m^{-2} s^{-1} of the measured fluxes at CR and $\sim$1.8 μmol m^{-2} s^{-1} of those at SOJP, with no significant differences among models. Regression statistics for CO_2 fluxes at both sites were adversely affected by large effluxes measured but not modelled during some nights (e.g. DOY 173, 176 and 177 in Fig. 5 (effluxes >20 μmol m^{-2} s^{-1} not plotted) and DOY 188 and 189 in Fig. 6).

4.7. Annual ecosystem C balances

Although CO_2 fluxes measured and estimated from eddy covariance were simulated with comparable accuracy by most of the models (Table 4), yearly aggregates of modelled fluxes differed markedly (Table 5a). Model ranking for annual *GPP* ($=\Sigma_t V_c$ where *t* = time steps in a year) and $R_a + R_h$ corresponded to that for summer daily *NEP* (Table 3) and annual CO_2 fluxes (Table 4). Lower *GPP* and $R_a + R_h$ from C-CLASSa, EALCO and CTEM at CR were close to those calculated by Morgenstern et al. (2004a) from gap-filled eddy covariance data using a threshold friction velocity (u^*_{th}) of 0.3 m s^{-1} for acceptance of fluxes, and no correction for incomplete energy balance closure (Table 5). Higher *GPP* and $R_a + R_h$ from BEPS, *ecosys* and C-CLASSm were closer to that estimated by Morgenstern et al. (2004a) with a 12% correction for incomplete energy balance closure. Total R_a among the models varied with *GPP* (through A.4.5) so that *NPP* ($=GPP - R_a$) from all models was close to the range of 370–640 g C m^{-2} y^{-1} (above-ground) and 770–890 g C m^{-2} y^{-1} (total) estimated by Keyes and Grier (1981) for two 40-year-old Douglas fir stands in nearby Washington State, USA.

The allocation of *NPP* between growth (A.4.5, A.4.6) and litterfall (A.4.7, A.4.8) at CR varied more widely among the models than did *NPP* itself, reflecting greater uncertainty in modelling processes of growth, allocation and senescence than in modelling those of C fixation and respiration. BEPS and C-CLASSa allocated most of *NPP* to litterfall leaving little for net growth, whereas *ecosys*, C-CLASSm and EALCO allocated about one-half of *NPP* to litterfall, leaving a similar amount for net growth. Bole growth rates of similarly aged Douglas fir stands measured in the study area were 12 m^3 ha^{-1} y^{-1} or 250–300 g C m^{-2} y^{-1}, indicating that Δ wood C in BEPS and EALCO were likely too low and too high respectively. R_h among the models varied with *NPP* (through litterfall effects on R_h in A.5.1 or on decomposition in A.5.10), so that *NEP* ($=NPP - R_h$) from all models except C-CLASSa were within 90 g C m^{-2} of *NEP* estimated from eddy covariance data. This value was estimated by Morgenstern et al. (2004a) to be the systematic bias in annual *NEP* due to methods of data analysis used to calculate eddy covariance fluxes. In some models, underestimation of daily *NEP* during July and August (Figs. 7 and 8) was offset by overestimation during May and June, indicating the importance of testing for seasonal trends in CO_2 exchange.

GPP from C-CLASSa and C-CLASSm at SOJP were markedly larger than that estimated from gap-filled eddy covariance fluxes (Table 5b), even though slopes from the regression of modelled on measured fluxes for these models were close to 1 (Table 4b).

Table 5
Annual C balances estimated from site measurements and modelled at (a) Campbell River (CR) and (b) Southern Old Jack Pine (SOJP) during 2000

	Estimated[a] ($g C m^{-2}$)	BEPS ($g C m^{-2}$)	*Ecosys* ($g C m^{-2}$)	C-CLASSa ($g C m^{-2}$)	C-CLASSm ($g C m^{-2}$)	EALCO ($g C m^{-2}$)	CTEM ($g C m^{-2}$)
(a) CR							
GPP	2120	2474	2590	2076	2504	2000	2151
R_a							
Above		837	1586	641	1121	659	
Below		680	276	473	426	436	
Total		1517	1862	1114	1547	1095	1348
NPP							
Above		420	460			546	
Below		425	268			360	
Total		957	728	962	957	906	803
Litterfall							
Above		437	193	217	158	122	
Below		362	65	548	206	368	
Exudation			122	184			
Total		799	383	949	364	490	
R_h		567	348	725	608	519	483
$R_a + R_h$	1730	2084	2210	1839	2155	1614	1831
Δ wood C		94	353	214	378	417	
Δ soil C			24	42	33		
NEP	390	390	380	237	349	388	320
LAI late June			8.5				
(b) SOJP							
GPP	557	765	792	1028	1207	660	758
R_a							
Above		281	293	337	423	298	
Below		188	142	229	244	134	
Total		469	435	566	667	432	493
NPP							
Above		177	203			108	
Below		119	154			121	
Total		296	357	462	540	229	265
Litter							
Above		148	141	143	105	67	
Below		103	81	258	107	119	
Exudation		n/a	69	135	n/a	n/a	*n/a*
Total		252	291	536	212	186	
R_h		177	271	378	455	146	166
$R_a + R_h$		646	706	944	1122	578	659
Δ wood C		39	60	92	206	42	
Δ soil C			64	0	74		
NEP	66	118	86	84	85	82	99
LAI late June			2.2				

[a] CR from Morgenstern et al. (2004a), SOJP from Griffis et al. (2003) using $u^*_{th} = 0.3\,m\,s^{-1}$ and no correction for energy balance closure.

GPP from BEPS, *ecosys*, EALCO and CTEM were closer to estimated values although slopes from the regression of modelled on measured fluxes for these models were less than 1 (Tables 3b and 4b). The low *GPP* modelled by EALCO at SOJP was consistent with low modelled versus measured CO_2 fluxes (Fig. 6e, Table 4b) and daily *NEP* (Table 3b), and may be attributed to low V_{rmax} in A.1.1. R_a among the models at SOJP varied with *GPP* as did those at CR. Thus *NPP* from C-CLASSa and C-CLASSm greatly exceeded a *NPP* of 226 g C m^{-2} measured by Gower et al. (1997) and Steele et al. (1997) at SOJP in 1994 which was climatically similar to 2000.

All models except C-CLASSm allocated most *NPP* to litterfall (A.4.7, A.4.8) at SOJP, leaving little for net growth. Wood growth rates in all models except C-CLASSm were consistent with ones of 57 and 59 g C m^{-2} y^{-1} measured at SOJP in 1993 and 1994 by Gower et al. (1997). As at CR, R_h among the models varied with *NPP* so that *NEP* from all models were within 30 g C m^{-2} of that estimated from gap-filled eddy covariance fluxes, except that from BEPS which was higher because of comparatively low R_h (Fig. 6a).

In a mature, undisturbed forest, Δ soil C (including DOC) is likely to be small in comparison to litterfall, and should equal total litterfall – R_h – Δ DIC (dissolved inorganic C) – (DOC + DIC) lost by runoff and leaching. Because only *ecosys* accounted for DOC (A.5.1) and DIC, these terms were omitted from Table 5. For the other models, Δ soil C should have equalled total litterfall – R_h. However in some models total litterfall $-R_h$ was larger (BEPS and C-CLASSa) or smaller (C-CLASSm) than likely values for Δ soil C at both sites, indicating that R_h had not equilibrated with litterfall during model spin up. Such equilibration needs to be achieved before future model tests of R_h.

5. Discussion

5.1. Modelled CO_2 and energy exchange under contrasting temperature and vapor pressure deficit

Changes from cool to warm T_a (>25 °C) and low to high *D* (>2 kPa) caused both the temperate Douglas fir stand at CR (Fig. 7) and the boreal jack pine stand at SOJP (Fig. 8) to change from a daily sink to a daily source of CO_2 on several occasions during the summer of 2000. During these periods, θ remained above the field capacities of the soils at both sites, so that changes in net CO_2 exchange were attributed to atmospheric rather than soil water status. The ability of the models in this study to simulate the magnitude of this change therefore depended upon their ability to simulate:

(1) the effects of *D* on g_l (A.2.1) and thereby on V_l (A.1.13). All the models in this study simulated the effects of *D* on g_l, either directly through *D* or indirectly through ψ_c (*ecosys*). However only *ecosys* and C-CLASSm explicitly modelled the effects of g_l on V_l, so that these two models more fully reproduced the magnitude of the sink – source transitions measured during warming events (Figs. 5-8; $b \rightarrow 1$ in Table 4). Both these models were able to simulate the steep declines in diurnal water use efficiency (WUE) measured under rising *D* at both sites (Fig. 9a and b) – C-CLASSm perhaps too much so. These declines indicated that comparative effects of g_l on V_l and *LE* were accurately modelled under changing *D*. Models that relied only on functions of ψ_s to constrain g_l, or of ψ_c

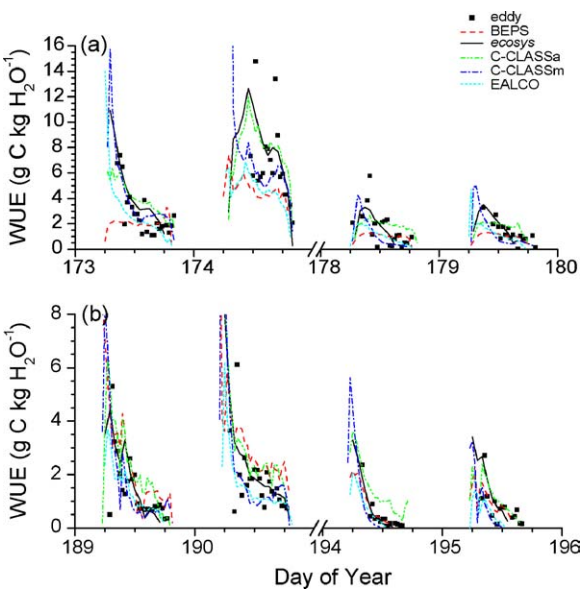

Fig. 9. Water use effeciency (WUE), calculated from CO_2 influxes divided by *LE* effluxes, measured by eddy covariance (symbols) and modelled (lines) during two days with lower (left) and higher (right) vapor pressure deficit *D* at (a) Campbell River and (b) Southern Old Jack Pine during summer 2000.

(C-CLASSa, EALCO) or θ (CTEM) to constrain V_l (A.1.4) generally did not simulate the depressing effect of high D on midafternoon CO_2 influxes. These models also simulated the steep declines in diurnal WUE, but these were sometimes less than measured (e.g. C-CLASSa in Fig. 9a and b). These functions likely need to be made more sensitive to D in conifers because of their low axial hydraulic conductivity (A.6.6). Models that used empirical formulations of g_l (BEPS) underestimated diurnal declines in WUE if these formulations were not sensitive enough to D (Fig. 9a), but simulated these declines better if they were (Fig. 9b). Explicit modelling of the effects of g_l on V_l should be considered in future model development.

(2) the effects of soil and air temperatures on V_l (A1.2, A1.8), R_a (A.4.2, A.4.4) and R_h (A.5.2, A.5.11). Peak CO_2 influxes were measured and modelled around 15–18 °C at CR (Fig. 10) and SOJP (Fig. 11). CO_2 influxes modelled by BEPS appeared to rise too rapidly at lower temperatures, most notably at CR (Fig. 10a), in spite of the adequate Q_{10} term in A1.2. Models that used Arrhenius functions in A1.2 (*ecosys*, C-CLASSa, EALCO) simulated rises in CO_2 influxes with temperature that were more gradual at CR (Fig. 10b,c,e), and perhaps too gradual at SOJP (Fig. 11b,c,e). Sharp declines in peak CO_2 influxes modelled and measured above 18 °C were attributed to D effects on g_l, most notably the declines in C-CLASSm (Figs. 10d and 11d) in which D effects were the most pronounced (Figs. 5d and 6d). The temperature sensitivity of $R_a + R_h$ derived from nighttime eddy covariance measurements was greater than that in most of the models. Morgenstern et al. (2004a) derived a Q_{10}

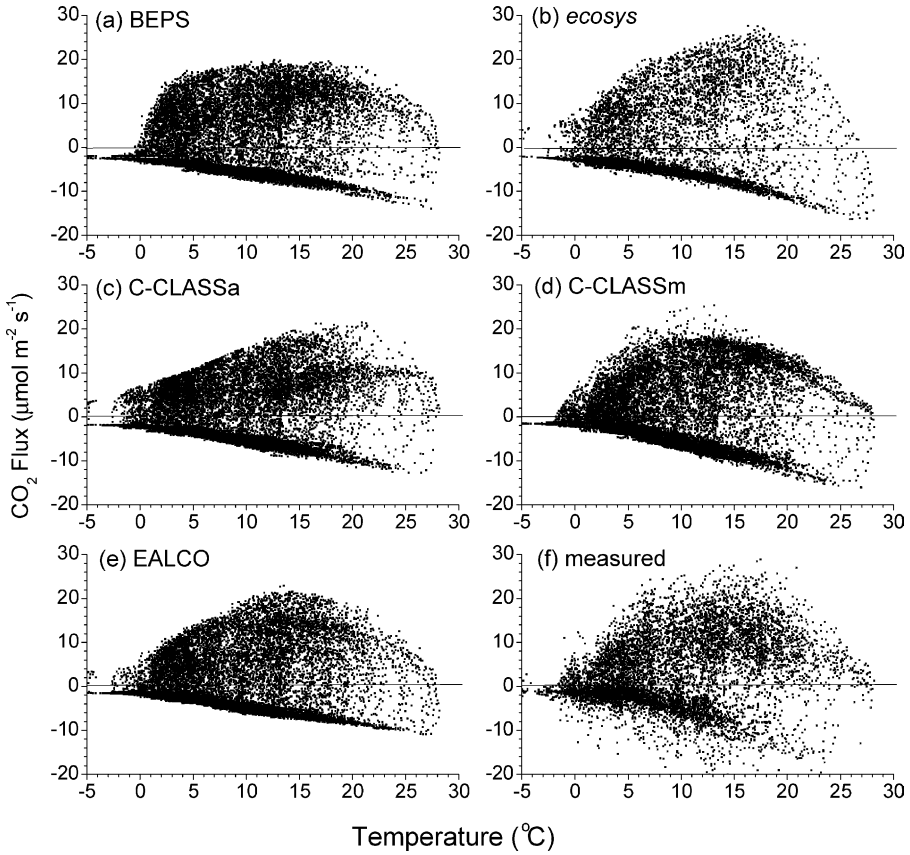

Fig. 10. Net CO_2 exchange vs. air temperature modelled (a–e) and measured by eddy covariance (f) at Campbell River during 2000. Downward fluxes were assigned positive values, and upward fluxes negative values.

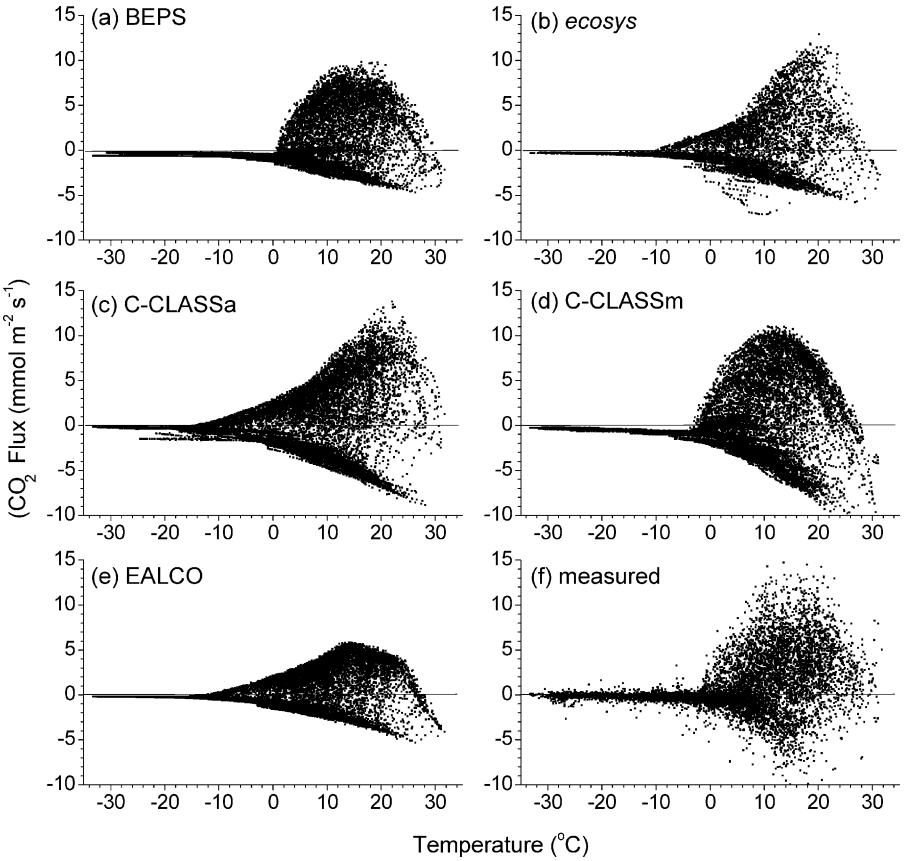

Fig. 11. Net CO_2 exchange vs. air temperature modelled (a–e) and measured by eddy covariance (f) at Southern Old Jack Pine during 2000. Downward fluxes were assigned positive values, and upward fluxes negative values.

of 5.1 with T_s at 5 cm when $u^* > 0.3\,m\,s^{-1}$ at CR in 2000. Griffis et al. (2003) derived a Q_{10} of 3.6 with T_s at 2cm when $u^* > 0.35\,m\,s^{-1}$ at SOJP in 2000. These large values of apparent Q_{10} may partly be attributed to the larger variation of T_a versus T_s that drove above-ground R_a. However these values suggest that underestimation of rises in $R_a + R_h$ with temperature by some models (e.g. EALCO in Figs. 5e and 6e) may have been caused by low Q_{10} for R_m (A.4.4) and in some cases R_h (A.5.2). This underestimation was apparent in the smaller rises of CO_2 effluxes with temperature modelled by EALCO at CR (Fig. 10e) and SOJP (Fig. 11e). The larger rise of R_h with T_s in *ecosys* (Fig. 5b) was attributed to higher-order effects of more rapid R_h (A.5.1) driving more rapid growth of active microbial biomass (M_a in A.5.7 from R_g in A.5.6), driving more rapid decomposition (A.5.8) and DOC production, in turn driving more rapid R_h (A.5.1) (Figs. 10b and 11b). Among first-order models of R_h, the larger rise of R_h with soil temperature in C-CLASSm (Figs. 5d, 6d, 10d, 11d) was driven by larger Q_{10} for R_h (A.5.2), and in C-CLASSa (Figs. 5c, 6c, 10c, 11c) by an Arrhenius function with an offset for cold-temperature adaptation that allowed R_h to rise more rapidly at lower temperatures (A.5.2). Appropriate, and in some cases greater, sensitivity of R_h and R_a to temperature needs to be considered in future model development.

5.2. *Limitations of eddy covariance measurements in evaluating model performances*

The confidence with which inferences can be drawn from the comparison of modelled and measured fluxes

(Figs. 3–8; Tables 3 and 4) depends upon uncertainty in the measured fluxes. This uncertainty may be attributed to two causes:

(1) Eddy covariance measurements are most accurate under turbulent, well-mixed conditions, but likely underestimate CO_2 and energy fluxes under the stable boundary layers that frequently develop during nighttimes. Fluxes recorded under stable conditions (defined here as $u^*_{th} < 0.3\,ms^{-1}$) were therefore excluded from comparison with modelled fluxes (Table 4). These fluxes were replaced by estimates based on relationships with key drivers (solar radiation, soil temperature) when $u^* > u^*_{th}$ to derive daily (Table 3) and yearly (Table 5) fluxes (see Barr et al., 2002 for details). Because replacement was required more frequently during nights, tests of modelled CO_2 effluxes versus temperature were less constrained than were those of CO_2 influxes.

(2) Incomplete recovery by eddy covariance of absorbed radiant energy ($R_n - G$) as dissipated heat ($LE + H$) has been proposed by Twine et al. (2000) to correspond with incomplete measurement of CO_2 fluxes. Recoveries of 0.88 at CR and 0.85 at SOJP indicated that LE and CO_2 fluxes may have been 13% and 17% larger than those measured. Although the need to replace CO_2 fluxes measured under low u^* is generally accepted, the need to correct CO_2 fluxes for incomplete recovery of heat energy is not. Therefore this correction was not applied to the hourly fluxes or their daily and annual totals used for model testing (Tables 3–5). Regressions of modelled on measured fluxes should therefore have given slopes (b in Table 4) of greater than one, and certainly not of much less than one.

When comparing eddy covariance measurements to other estimates of NEP on half-hourly to annual scales, it is important to take into account three different sources of uncertainty: (1) the random error of the flux measurements that is due to the statistical nature of the turbulent transport process, (2) the systematic error of the flux measurement that is due to differences in instrument gains, systematic biases due to signal attenuation, etc., and (3) systematic differences in the gap filling algorithm that is applied to derive annual totals of NEP from an incomplete record of half-hourly EC measurements.

The random error is commonly assumed to be less than 20% (Wesely and Hart, 1985) and because of its random nature it makes only a minor contribution to uncertainty of annual totals of NEP (Morgenstern et al., 2004a). The systematic error was evaluated by intercomparisons between two independent eddy covariance systems at four FCRN sites with eddy covariance systems, calibration procedures and equipment maintenance standards very similar to those at CR and SOJP (Morgenstern et al., 2004b). For all four sites, turbulent fluxes of H, LE and CO_2 agreed to within 5%. Since this is a systematic difference between measurements, this uncertainty would also be present in the annual sum. In other studies, uncertainties from lack of turbulence and incomplete energy recovery, combined with those from gas sampling and measurement, contributed to standard errors of $38\,W\,m^{-2}$ for LE measured by eddy covariance over grassland (Twine et al., 2000), and the greater of 15–20% or $30\,W\,m^{-2}$ for that over deciduous forests (Wilson and Baldocchi, 2000). These values were comparable to root mean squares for differences (RMSD) between modelled and measured LE at both CR (29–33 $W\,m^{-2}$) and SOJP (27–40 $W\,m^{-2}$). Comparisons with eddy covariance fluxes at an annual time scale were thus unable to distinguish among the accuracies with which mass and energy exchange were simulated by the different models in this study. However these comparisons did indicate that variation with weather in LE and CO_2 fluxes was underestimated by >20% ($b < 0.8$) by C-CLASSa at CR, and by BEPS, C-CLASSa (LE only), EALCO and CTEM at SOJP.

The comparison of annual *NEP* calculated by the models and estimated from measurements (Table 5) must be evaluated with respect to uncertainty in annual *NEP* estimated from measurements. These estimates required that CO_2 fluxes recorded when $u^* < u^*_{th}$ be replaced by fluxes estimated from relationships derived under more turbulent conditions. CO_2 effluxes were more frequently replaced than were CO_2 influxes with values that were frequently larger than those recorded, so that apparent $R_a + R_h$ rose with values selected for u^*_{th}. Morgenstern et al. (2004a) found that raising u^*_{th} from 0.2 to $0.3\,m\,s^{-1}$ lowered annual *NEP* estimated at CR by $90\,g\,C\,m^{-2}$. Griffis et al. (2003) found that applying a u^*_{th} of $0.35\,m\,s^{-1}$ reduced *NEP* estimated at SOJP by $38\,g\,C\,m^{-2}$. On the other hand, correcting for incomplete energy recovery would have raised CO_2 influxes more than CO_2 effluxes because influxes were

usually larger. This correction would have raised estimated *NEP* by 30 g C m^{-2} from that reported at CR (Morgenstern et al., 2004a) and by 12 g C m^{-2} from that at SOJP (Griffis et al., 2003). The uncertainty of annual NEP was estimated to be about 25% at a nearby FCRN deciduous site, depending on the distribution of gaps over the year and the treatment of energy balance closure (Griffis et al., 2003). Differences between modelled and estimated annual *NEP* would have to be larger than differences caused by assumptions in the estimated values before model divergence from measurements could be inferred.

5.3. Comparison with other modelling of eddy covariance measurements

The competence of the ecosystem models in this study to simulate CO_2 and energy fluxes was comparable with that of more specialized models that have been adapted to similar site conditions. The mass and energy exchange model of Kellomäki and Wang (1999, 2000) used site-specific parameterizations of soil thermal properties, soil respiration, soil surface resistance to evaporation, plant hydraulic resistance, photosynthetic capacity (V_{rmax} and J_{max} from prescribed foliar N), and of g_l and its responses to environment. When parameterized at a boreal Scots pine (*Pinus sylvetris* L.) site, this model reproduced 72% ($b = 1.06$) and 61% ($b = 0.51$) of variation in half-hourly measurements of daytime and nighttime CO_2 fluxes respectively, and 76% ($b = 1.08$) of those in vapor fluxes, during 19 summer days with low D and high θ. Arneth et al. (1998) developed a biophysical model of CO_2 fixation and respiration with parameters (V_{rmax}, J_{max} and soil respiration) derived from eddy covariance and surface CO_2 fluxes. When parameterized at a temperate radiata pine (*Pinus radiata* L.) plantation, this model reproduced 53% ($b = 0.77$) and 59% ($b = 0.84$) of variation in hourly CO_2 fixation and respiration respectively measured during 14 days over 2 growing seasons. These performances were equalled or exceeded by most of the models in this study, which were parameterized independently of site measurements, at CR (Table 4a) and SOJP (Table 4b), during entire years with large variation in D and some variation in θ.

The competence of the models in this study to simulate daily *NEP* also compared well with that of other models. Law et al. (2000b) parameterized the multi-layer biosphere-atmosphere gas exchange models CANPOND (Baldocchi and Meyers, 1998) and SPA (Williams et al., 1996) from seasonal measures of soil respiration, temperature and water content, LAI and maximum leaf CO_2 fixation rates (V_{rmax} and J_{max}) at a semiarid, temperate ponderosa pine (*Pinus ponderosa*) site. CANPOND reproduced 30 and 2% of variation in daily *NEP* measured by eddy covariance during 2 years, while SPA reproduced 49 and 28%. The models in this study reproduced 42–87% of variation in daily *NEP* measured by eddy covariance at CR (Table 3a; Fig. 7), and 12–52% of that at SOJP (Table 3b; Fig. 8), indicating ongoing progress in reconciling modelled with measured *NEP*.

These results indicate that the performances of comprehensive, generally applicable ecosystem models can approach those of specialized, site-specific models. These results also indicate that 20% or more of variance in CO_2 and energy fluxes measured by eddy covariance remain unexplained by models, even those with detailed mass and energy transfer schemes. This variance is likely caused by minute-scale micrometeorological phenomena which create scatter in the measured fluxes not associated with the half-hourly to hourly changes in the boundary conditions that drive modelled fluxes. It may also be explained by the random error of the flux measurements due to the statistical nature of the turbulent transport process, commonly assumed to be less than 20% (Wesely and Hart, 1985). This unexplained variance limits the extent to which eddy covariance data can be used to discriminate among alternative model hypotheses.

Acknowledgements

The Fluxnet-Canada Research Network is funded by the Natural Sciences and Engineering Research Council of Canada (NSERC), the Canadian Foundation for Climate and Atmospheric Sciences (CFCAS), and the Biological Implications of CO_2 Policy in Canada (BIOCAP). Computational facilities for *ecosys* were provided by the Multimedia Advanced Computational Initiative (MACI) at the Universities of Alberta and Calgary.

Appendix A

Key algorithms used in the models (N/A = not applicable or available)

	BEPS	*ecosys*	C-CLASSa	C-CLASSm	EALCO	CTEM
A.1 CO_2 fixation						
A.1.1 maximum rubisco-limited CO_2 fixation rate V_{rmax}	60 μmol m^{-2} s^{-1} at 25°C for all forest types	40 μmol g^{-1} activated rubisco s^{-1} at 25 °C for all C_3 plants	90 μmol m^{-2} leaf area s^{-1} at24 °C (SOJP) or at 27 °C (CR) when leaf structural N > 70 g kg^{-1} structural C	49 μmol m^{-2} leaf area $s^{-1}-$ at 25 °C and top of canopy ($V_{rmax(0)}$) for sunlit leaves: $V_{c\,max(0)}\,\frac{1-\exp(-(k_N+k_b)L)}{k_N+k_b}$ for shaded leaves: $V_{c\,max(0)}\left\{\frac{1-\exp(-k_N L)}{k_N}-\frac{1-\exp(-(k_N+k_b)L)}{k_N+k_b}\right\}$ k_N = foliar nitrogen content decay coefficient (0.14) k_b = beam radiation extinction coefficient L = LAI	30 μmol m^{-2} leaf area s^{-1} at 25 °C and leaf C:N = 20	60 μmol CO_2 m^{-2} leaf area s^{-1} at 25 °C
A.1.2 temperature effect on rubisco-limited CO_2 fixation rate V_r	$2.3^{25-T/10}$	Arrhenius function of canopy temperature: E_a = 57.5 kJ mol^{-1} with low and high temperature inactivation and offset of +4.5 °C at SOJP and +3.0 °C at CR	Arrhenius function of canopy temperature: E_a = 57.5 kJ mol^{-1} with low and high temperature inactivation and optimum of 24.0 °C at SOJP and +27 °C at CR	$\left(\frac{T_{leaf}-T_{min}}{T_{opt}-T_{min}}\right)\left(\frac{T_{max}-T_{leaf}}{T_{max}-T_{opt}}\right)$, T_{min} = −2 °C, T_{opt} = 35 °C, T_{max} = 50 °C	Arrhenius: E_a = 57.5 kJ mol^{-1}. Optimum temperature set at 20 °C	$\frac{f_{25}(Q10)}{\{[1+\exp\{0.3(T_c-T_{up})\}]\,[1+\exp\{0.3(T_{low}-T_c)\}]\}}$, $f_{25}(Q_{10}) = Q_{10}^{0.1(T_c-25)}$, T_{low} is −5 °C, T_{up} is 34 °C
A.1.3 nitrogen effect on V_r	0.75 for coniferous forests 1.0 for broadleaf forests	Rubisco concentration = f(leaf structural N:C) rubisco activation = f(leaf non-structural N:C)	f (leaf structural N:C), modified by f (leaf non-structural N:C)	N/A	V_{rmax} −2 (C:N-20) range 10–45	N/A
A.1.4 water effect on V_r	Through effect on g_c in A.2.2	$f(e^{-b\psi_T})$, b = 3, $\psi_T = \psi_c - \psi_\pi$	$(\exp(\mu_w(\psi_c-\psi_0)/(10RT_c))^{30}$, ψ_0 = −80 m, μ_w = 0.018 kg mol^{-1}, R = 8.314 J mol^{-1} K^{-1}	$\min\left(1, \frac{3(\theta_s-\theta_{min})}{\theta_{max}-\theta_{min}}\right)$, θ_s = root zone θ, θ_{min} = minimum θ (0.05), θ_{max} = porosity	(COS($\pi\psi_c/\psi_{max}$) + 1.0)/2.0, ψ_{max} = −350 m	$1.0-(1.0-\beta)^n$, n = 2, $\beta(\theta)$ = $\max\left[0, \min\left(1, \frac{\theta-\theta_{wilt}}{\theta_{field}-\theta_{wilt}}\right)\right]$
A.1.5 CO_2 effect on V_r	$30 \times 2.1^{25-t/10}$ pa	K_m = 12.5 μM	K_m = 12.5 μM		K_m = 12.5 μM	N/A
A.1.6 maximum electron transport rate J_{max}	J_{max} = 29.1 + 1.64 × V_{cmax}	360 μmol g chlorophyll s^{-1} at 25 °C for all C_3 plants	180 μmol m^{-2} leaf area s^{-1} at 24 °C (SOJP) or at 27 °C (CR) and leaf structural N > 70 g kg^{-1} structural C	2.7 × V_{rmax}	50 μmol m^{-2} leaf area s^{-1} at 25 °C	N/A
A.1.7 irradiance effect on electron transport rate J	$\frac{J_{max}I}{I+2.1J_{max}}$	$(QI+J_{max}-((QI+J_{max})^2-4\alpha QIJ_{max})^{0.5})/2\alpha$, Q = 0.45 μmol μmol^{-1}, α = 0.75	$(QI+J_{max}-((QI+J_{max})^2-4\alpha QIJ_{max})^{0.5})/2\alpha$, Q = 0.45 μmol μmol^{-1}, α = 0.8	$(QI+J_{max}-((QI+J_{max})^2-4\alpha QIJ_{max})^{0.5})/2\alpha$, Q = 0.20 μmol μmol^{-1}, α = 0.7	$J=\{QI+J_{max}-[(QI+J_{max})^2-4\alpha QIJ_{max}]^{0.5}\}/2\alpha$; Q = 0.45 μmol μmol^{-1} = 0.8	$Q(1-\varpi)I$, Q = 0.40μmol μmol^{-1}, ϖ = scattering coefficient
A.1.8 temperature effect on J	As for V_{rmax} in A.1.2	As for V_{rmax} in A.1.2	As for V_{rmax} in A.1.2	As for V_{rmax} in A.1.2	As for V_{rmax} in A.1.2	As for V_{rmax} in A.1.2
A.1.9 nitrogen effect on J	As for V_{rmax} in A.1.3	Chlorophyll concentration = f(leaf structural N:C), chlorophyll activation = f(leaf non-structural N:C)	As for V_{rmax} in A.1.3	As for V_{rmax} in A.1.3	J_{max} − 5 (C:N-20) range 20–120	As for V_{rmax} in A.1.3

Appendix A (*Continued*)

	BEPS	*ecosys*	C-CLASSa	C-CLASSm	EALCO	CTEM
A.1.10 water effect on J	N/A	As for V_{rmax} in A.1.4	As for V_{rmax} in A.1.4	As for V_{rmax} in A.1.4	As for V_{rmax} in A.1.4	
A.1.11 quantum efficiency ε	$(C_i - \Gamma^*)/(4.5\ C_i + 10.5\Gamma^*)$	$(C_i - \Gamma^*)/(4.5\ C_i + 10.5\Gamma^*)$	$(C_i - \Gamma^*)/(4.5\ C_i + 10.5\Gamma^*)$	$\frac{(C_i-\Gamma^*)}{4(C_i+2\Gamma^*)}$	$(C_i - \Gamma^*)/(4.5\ C_i + 10.5\Gamma^*)$	
A.1.12 light-limited CO_2 fixation rate V_j	$J\varepsilon$	$J\varepsilon$	$J\varepsilon$	$J\varepsilon$	$J\varepsilon$	
A.1.13 leaf CO_2 fixation rate V_l	$\min(V_r,V_j)$ - R_d: R_d = dark respiration	Iterative solution for C_i such that: $\min(V_r,V_j) = g_l (C_a - C_i)$	$\min(V_r,V_j)$	Iterative solution of: $\min(V_r,V_j) - R_d = g_c (C_a - C_i)$, R_d = dark respiration	$\min(V_r,V_j)$	$\beta_1 V^2 - V(V_r + V_j) + V_r V_j = 0$, $\beta_2 A^2 - A_0(V + V_s) + VV_s = 0$, β_1 and β_2 = curvature coefficients >0.9 and <0.99, V = smoothed average of V_r and V_j, A = smoothed average of V and the capacity to export or utilize photosynthesis products (V_s)
A.2 stomatal conductance						
A.2.1 leaf conductance g_l	$g_l = 1/r$, $r = r_{min} f(T) f(D) f(\psi) f(R)$, $f(T) = \frac{1}{1-0.0016(25-T)^2}$, $f(D) = 1/(1 + 2.29D)$ (CR), $f(D) = (0.161–0.068)(1 + 0.355D)/(0.161–0.068(1 + 0.355D))$ (SOJP) $f(\psi) = \sum_{i=1}^{4} f(\psi_i) w_i$, $w_i = \frac{R_i/\psi_i}{\sum_{i=1}^{4} R_i/\psi_i} w_i$ is the root fraction in layer i $f(R) = \frac{1000}{1000+R_{min}} \frac{R+R_{min}}{R}$, $R_{min} = 30$	$g_{lmax} = V_l/(C_a - C_i)$	$g_{lmin} + mV_l H/C_a$, $g_{lmin} = 0.0001\ m\ s^{-1}$, $m = 6$, H = RH	$g_{lmin} + mf_w V_l/\{(C_i - \Gamma)(1 + D/D_0)\}$, $g_{lmin} = 0.01\ mol\ m^{-2}\ s^{-1}$, $m = 3$, f_w from θ as in A.1.4, D_0 = 2 kPa (CR), 4 kPa (SOJP)	$g_{lmin} + mV_l H/C_a$, $g_{lmin} = 0.0001\ m\ s^{-1}$, $m = 9$, H = RH	N/A
A.2.2 water effect on g_l	if $\psi < -100$ kPa, $f(\psi i) = 1 + \left(\frac{-\psi i - 100}{100}\right)^{0.75}$, else, $f(\psi_1) = 1$, ψ = soil water potential (kPa)	$r_l = r_{lmin} + (r_{lmax} - r_{lmin}) e^{-b\psi_T}$, $r_l = g_l^{-1}$ from A.2.1, $r_{lmin} = g_{lmax}^{-1}$ from A.2.1, $\psi_T = \psi_c - \psi_\pi$, $b = 5$	Through water effect on V_r, V_j in A.1.4	Through θ on V_r, V_j in A.1.4 and on g_l in A.2.1	Through water effect on V_r, V_j in A.1.4	Through water effect on V_r, V_j in A.1.4
A.2.3 canopy conductance g_c	$g_{l,sunlit}\ A_{l,sunlit} + g_{l,shaded}\ A_{l,shaded}$	$\sum g_l A_l$: A_l is the area of leaf surface with spatial resolution defined below	$g_{l,sunlit}\ A_{l,sunlit} + g_{l,shaded}\ A_{l,shaded}$	$g_{l,sunlit}\ A_{l,sunlit} + g_{l,shaded}\ A_{l,shaded}$	$g_{l,sunlit}\ A_{l,sunlit} + g_{l,shaded}\ A_{l,shaded}$	$g_{cmin} + mA_n p/\{(C_i - \Gamma)(1+D/D_0)\}$, $g_{cmin} = 0.01\ mol\ m^{-2}\ s^{-1}$, $A_n = A -$ leaf respiration, p = surface pressure (Pa) $m = 6$, $D_0 = 2$ kPa
A.2.4 leaf spatial resolution	Sunlit and shaded fractions depending on solar zenith angle	Species, branch, layer, node, azimuth, inclination, sunlit vs. shaded depending on solar zenith angle, clumping	Sunlit and shaded fractions depending on solar zenith angle	Sunlit and shaded fractions depending on solar zenith angle	Multilayer with explicit crown shape and stand distribution, sunlit vs. shaded	Big leaf, or sunlit and shaded fractions depending on solar zenith angle
A.3 nitrogen						
A.3.1 maximum N uptake	N/A	1.4×10^{-6} g NH_4^+ or NO_3^- m^{-2} root area s^{-1} at 25NH_4^+ °C	1.4×10^{-6} g N m^{-2} root area s^{-1} at 24 °C (SOJP) or at 27 °C (CR)	N/A	1.4×10^{-6} g N m^{-2} root area s^{-1} at 25 °C	N/A
A.3.2 soil N effect on N uptake	N/A	K_m = 0.35 g NH_4^+ or NO_3^- m^{-3} water	K_m = 0.35 g N m^{-3} water	N/A	K_m = 0.35 g N m^{-3} water	N/A

Appendix A (*Continued*)

	BEPS	*ecosys*	C-CLASSa	C-CLASSm	EALCO	CTEM
A.3.3 soil temperature effect on N uptake	N/A	Arrhenius function of root temperature: $E_a = 57.5\,kJ\,mol^{-1}$ with low and high temperature inactivation and offset of +4.5 °C at SOJP and +3.0 °C at CR	Arrhenius function of root temperature: $E_a = 57.5\,kJ\,mol^{-1}$ with low and high temperature inactivation and optimum of 24.0 °C at SOJP and 27 °C at CR	N/A	Arrhenius: $E_a = 57.5\,kJ\,mol^{-1}$	N/A
A.3.4 plant N effect on N uptake	N/A	NH_4^+ or NO_3^- uptake = f (root non-structural C:N:P)	f (root non-structural C:N)	N/A	f (root N concentration)	N/A
A.3.5 plant N/C						
Leaves	N/A	0.05 max. (conifers), varies with leaf non-structural C:N:P ratio	0.0625 max., varies with shoot non-structural N:C ratio	N/A	0.047 varies with leaf C:N assimilation	N/A
Twigs	N/A	0.02	0.0167	N/A	0.016 varies with sapwood C:N assimilation	N/A
Roots	N/A	0.02	0.02	N/A	0.024 varies with root C:N assimilation	N/A
Wood	N/A	0.0025	0.00135	N/A	0.002	N/A
A.4 autotrophic respiration						
A.4.1 total autotrophic respiration R_a	$R_{gi} + R_{mi}$, R_g = growth respiration, R_m = maintenance respiration, i = leaf, wood or root	$R_a' C_n f(T) f(C_n : N_n)$, $R_a' = 4.17 \times 10^{-6}\,s^{-1}$ at 25 °C, C_n = non-structural C, N_n = non-structural N	$R_a' C_n f(T) f(C_n : N_n)$, $R_a' = 4.17 \times 10^{-6}\,s^{-1}$ at 24 °C (SOJP) or at 27 °C (CR), C_n = non-structural C, N_n = non-structural N	$R_{gi} + R_{mi}$, R_g = growth respiration, R_m = maintenance respiration, i = leaf, wood or root	$R_{gi} + R_{mi}$, R_g = growth respiration, R_m = maintenance respiration, i = leaf, wood or root	$R_{gi} + R_{mi}$, R_g = growth respiration, R_m = maintenance respiration, i = leaf, wood or root
A.4.2 temperature effect on R_a	Through effects on R_m, V_c	Arrhenius function of canopy or root temperature: $E_a = 57.5\,kJ\,mol^{-1}$ with low and high temperature inactivation and an offset of +4.5 °C at SOJP and +3.0 °C at CR	Arrhenius function of canopy or root temperature: $E_a = 57.5\,kJ\,mol^{-1}$ with low and high temperature inactivation and optimum of 24.0 °C at SOJP and 27 °C at CR	Through effects on R_m, V_c	Through effects on R_m, V_c	Through effects on R_m, V_c
A.4.3 maintenance respiration R_m	Leaf: $1.16 \times 10^{-7}\,gC\,g^{-1}\,C\,s^{-1}$ stem: $2.31 \times 10^{-8}\,gC\,g^{-1}\,C\,s^{-1}$, root: $1.74 \times 10^{-8}\,gC\,g^{-1}\,C\,s^{-1}$ at 25 °C	$3.2 \times 10^{-6}\,gC\,gN^{-1}\,s^{-1}$ at 25 °C	$2.3 \times 10^{-6}\,gC\,gN^{-1}\,s^{-1}$ at 25 °C	Leaf: $1.5 \times 10^{-5}\,gC\,m^{-2}$ area s^{-1} sapwood: $2.3 \times 10^{-9}\,gC\,g^{-1}\,C\,s^{-1}$ coarse root: $4.3 \times 10^{-9}\,g\,C\,g^{-1}\,C\,s^{-1}$ fine root: $1.14 \times 10^{-7}\,g\,C\,g^{-1}\,C\,s^{-1}$ at 25 °C	$2.06 \times 10^{-6}\,gC\,gN^{-1}\,s^{-1}$ at 25 °C	Leaf: 0.015 V_l (C_3) 0.025 V_l (C_4), wood: $1.37 \times 10^{-8}\,g\,C\,g^{-1}\,C\,s^{-1} \times lf_w$, root: $4.53 \times 10^{-8}\,g\,C\,g^{-1}\,C\,s^{-1} \times lf_f$ at 25 °C, $lf_{w,r} = \max(0.05, \min(\exp(-0.2835\,C_{w,r}), 1.0))$
A.4.4 temperature effect on R_m	$2.3^{T-25/10}$	$Q_{10} = 2.25$, based on canopy or root temperature	$Q_{10} = 2.0$, based on canopy or root temperature	$Q_{10,leaf} = 2.0$, $Q_{10,wood} = 1.7$, $Q_{10,root} = 1.9$, based on canopy or soil temperature	$Q_{10,leaf} = 2.1$, $Q_{10,wood} = 1.3$, $Q_{10,root} = 1.9$, based on canopy or soil temperature	$Q_{10} = 3.22 – 0.046T$
A.4.5 growth respiration R_g	0.2 V_c	$\max(0, R_a - R_m)$	$\max(0, R_a - R_m)$	0.15 $(V_c - R_m)$	0.24 $(V_c - R_m)$	$\max(0, 0.30\,(V_c - R_m))$
A.4.6 growth yields N/A						
Leaves	$4.0\,g\,C\,g\,R_g^{-1}$	$2.6\,g\,C\,g\,R_g^{-1}$	$2.44\,g\,C\,g\,R_g^{-1}$		0.57 of C used for leaf growth (=0.57/0.43???)	
Non-foliar	$4.0\,g\,C\,g\,R_g^{-1}$	$3.2\,g\,C\,g\,R_g^{-1}$	$2.44\,g\,C\,g\,R_g^{-1}$		0.57 of C used for sapwood growth	
Roots	$4.0\,g\,C\,g\,R_g^{-1}$	$3.2\,g\,C\,g\,R_g^{-1}$	$2.44\,g\,C\,g\,R_g^{-1}$		0.57 of C used for root growth	
Wood	$4.0\,g\,C\,g\,R_g^{-1}$	$4.0\,g\,C\,g\,R_g^{-1}$	Transformed from dead sapwood		Sapwood senescence-sapwood litterfall	

Appendix A (*Continued*)

	BEPS	*ecosys*	C-CLASSa	C-CLASSm	EALCO	CTEM
A.4.7 senescence respiration R_s	N/A	$\max(0, R_m - R_a)$	$\max(0, R_m - R_a)$		N/A	
A.4.8 litterfall	N/A	$R_s\,(1-F_s)/F_s$, F_s = fraction of leaf, twig or root C that is remobilizable	$R_s\,(1-F_s)/F_s$ + phenology-driven turnover, F_s = fraction of leaf, twig or root C that is remobilizable	sum of biomasses × prescribed turnover rates for leaf, wood and root	Phenology-driven turnover based on accumulated temperature	Turnover for leaf from specified life span of 2.5 year, and from cold and drought stress. Turnover for stem of 50 year and root of 7.6 year.
A.5 Heterotrophic respiration						
A.5.1 total heterotrophic respiration R_h	$D_c\,(1-\varepsilon)$, D_c = decomposition in A.5.8, ε = 0.4–0.7, depending on C pools	$R'_h M_a[C_d]/(K_r + [C_d]) f(T_s)$, $f(C:N:P)$, $R'_h = 3.125 \times 10^{-5}$ g C gmicr.C^{-1} s^{-1} at 25 °C, M_a = active microbial C g m^{-2}, $[C_d]$ = [DOC] g m^{-3}, K_r = 36 g C m^{-3}	$D_c\,(1-\varepsilon)$, D_c = decomposition in A.5.8, ε = 0.5 (CH_2O), 0.3 (cellulose), 0.2 (lignin), 0.4 (active SOC), 0.2 (slow SOC), 0.2 (humus)	$R_{litter} + R_{soil}$, $R_{soil} = R'_{soil}$ $C_s\,f(T_s)\,f(\theta_s)$, $R'_{soil} = 6.24 \times 10^{-8}$ g C g^{-1} C s^{-1} at 25 °C, C_s = SOC, $R_{litter} = R'_{litter}\,C_l\,f(T_s)\,f(\theta_s)$, $R'_{litter} = 9.60 \times 10^{-8}$ g C g^{-1} C s^{-1} at 25 °C, C_l = litter C, T_s = temperature of top soil layer (0–10 cm)	$D_c\,(1-\varepsilon)$, D_c = decomposition in A.5.8, ε = 0.5 (CH_2O), 0.3 (cellulose), 0.2 (lignin), 0.4 (active SOC), 0.2 (slow SOC), 0.2 (humus)	$R_{litter} + R_{soil}$, $R_{soil} = R'_{soil}$ $C_s\,f(T_s)\,f(\theta_s)$, $R'_{soil} = 1.95 \times 10^{-8}$ g C g^{-1} C s^{-1} at 25 °C, C_s = SOC, $R_{litter} = R'_{litter}\,C_l\,f(T_s)\,f(\theta_s)$, $R'_{litter} = 7.0 \times 10^{-8}$ g C g^{-1} C s^{-1} at 25 °C, C_l = litter C
A.5.2 temperature effect on R_h	$e^{308.56(1/35+46.032-1/T+46.32)}$	Arrhenius function of soil temperature: E_a = 57.5 kJ mol^{-1} with low and high temperature inactivation and an offset of +4.5 °C at SOJP and +3.0 °C at CR	Through effect on D_c in A.5.11	Q_{10} = 4.0	Through effect on D_c in A.5.11	$Q_{10} = \exp(2.04\,(1\text{-}T_s/T_{opt}))$, T_{opt} = 36.9 °C
A.5.3 water effect on R_h	Through the effect on decomposition (A.5.12)	$R'_h Q_{O_2}/Q'_{O_2}$ Q_{O_2} = O_2 uptake, Q'_{O_2} = O_2 demand	Through effect on D_c in A.5.12	$\{\theta/(0.5\theta_{FC} - \theta)\} \times \{0.5\theta_s/(0.5\theta_s + \theta)\}$, R_{soil} only), θ_{FC} = field capacity, θ_s = saturation	Through effect on D_c in A.5.12	$\max(0, \min(1, (1 - \{\log(\lvert\psi\rvert) - \log(\lvert\psi\rvert_{mn})\}/\{\log(\lvert\psi\rvert_{mx}) - \log(\lvert\psi\rvert_{mn})\})))$, $\lvert\psi\rvert_{mx}$ = 100 MPa $\lvert\psi\rvert_{mn}$ = 0.06 MPa
A.5.4 maintenance respiration R_m	N/A	3.33 × 10^{-6} g C g micr. N^{-1} s^{-1} at 25 °C	N/A	N/A	N/A	N/A
A.5.5 effect of temperature on R_m	N/A	Q_{10} = 2.25	N/A	N/A	N/A	N/A
A.5.6 growth respiration R_g	N/A	$\max(0, R_h - R_m)$	N/A	N/A	N/A	N/A
A.5.7 growth yield	N/A	1.5 g M_a g R_g^{-1} (aerobic)	N/A	N/A	N/A	N/A
A.5.8 decomposition D_c	$\sum K_{di} C_i f(T) f\left(\frac{\theta}{\theta_s}\right)$: K_d is the rate constant	$K_d\,M_a\,C_o/(C_o + K_c)\,f(T_s)$, K_d = rate constant, M_a = active microbial C, C_o = SOC, K_c = SOC at 1/2 D_{cmax}	$K_d\,C_o\,f(T_s)\,f(\psi_s)\,f(C_o{:}N_o)$, K_d = rate constant, C_o = SOC, N_o = SON	$K_d C_l$, K_d = rate constant, C_l = total litter C, calculated for litter C to SOC only	$K_d\,C_o\,f(T)\,f(\psi)\,f(\alpha_N)$, K_d = rate constant, C_o = SOC, α_N = C:N ratio	0.43 R_{litter} 0.43 R_{soil}
A.5.9 decomposition rate constants for soil pools K_{ds}	2.67 × 10^{-7} s^{-1} (surface microbe), 3.62 × 10^{-7} $(1 - F_{clay\ and\ silt})$ s^{-1} (soil microbe), 7.08 × 10^{-9} s^{-1} (slow), 1.43 × 10^{-10} s^{-1} (passive)	5.21 × 10^{-6} g C g M_a^{-1} s^{-1} (POC), 1.04 × 10^{-6} g C g M_a^{-1} s^{-1} (humus) at 25 °C	1.16 × 10^{-7} s^{-1} (active) 3.47 × 10^{-9} s^{-1} (slow), 9.28 × 10^{-12} s^{-1} (humus) at 24 °C (SOJP) or at 27 °C (CR)	N/A	1.16 × 10^{-7} s^{-1} (active) 3.47 × 10^{-9} s^{-1} (slow), 9.28 × 10^{-12} s^{-1} (humus) at 25 °C	N/A

Appendix A (*Continued*)

	BEPS	*ecosys*	C-CLASSa	C-CLASSm	EALCO	CTEM
A.5.10 decomposition rate constants for litter pools K_{dl}	$1.52 \times 10^{-7} \times e^{(-3L)}$ s^{-1} (leaf structural), 7.40×10^{-7} s^{-1} (leaf metabolic), $1.97 \times 10^{-7} \times e^{(-3L)}$ s^{-1} (leaf structural), 1.14×10^{-6} s^{-1} (leaf metabolic), $1.41 \times 10^{-7} \times e^{(-3L)}$ s^{-1} (woody), L = lignin content	2.08×10^{-4} g C g M_a^{-1} s^{-1} (protein, CH_2O), 3.125×10^{-5} g C g M_a^{-1} s^{-1} (cellulose), 5.21×10^{-6} g C M_a^{-1} s^{-1} (lignin), at 25 °C	2.56×10^{-6} s^{-1} (CH_2O), 3.67×10^{-7} s^{-1} (cellulose), 1.16×10^{-7} s^{-1} (lignin), at 24 °C (SOJP) or at 27 °C (CR)	N/A	2.56×10^{-6} s^{-1} (CH_2O), 9.67×10^{-7} s^{-1} (cellulose), 1.16×10^{-7} s^{-1} (lignin), at 25 °C	N/A
A.5.11 temperature effect on decomposition	$e^{308.56(1/35+46.032-1/T+46.32)}$	Arrhenius E_a = 57.5 kJ mol^{-1} with low and high temperature inactivation and an offset of +4.5 °C at SOJP and +3.0 °C at CR	Arrhenius E_a = 57.5 kJ mol^{-1} with low and high temperature inactivation and optimum of 24.0 °C at SOJP and 27 °C at CR	Q_{10} = 4.0	Arrhenius: E_a = 57.5 kJ mol^{-1}. optimum T = 35 °C	
A.5.12 water effect on decomposition	coarse soil $5.44\left(\frac{\theta}{\theta_s}\right) - 5.03\left(\frac{\theta}{\theta_s}\right)^2 - 0.472$, medium to fine soil $5.63\left(\frac{\theta}{\theta_s}\right) - 4.64\left(\frac{\theta}{\theta_s}\right)^2 - 0.710$	$K_c = K'_c\{1 + [M_a/\theta]/K'_i\}$, K'_c = 75 g C Mg^{-1}, K'_i = 25 g Cm^{-3}	$(\exp(\mu_w(\psi_c - \psi_0)/(10RT_c))^{30}$: $\psi_0 = -0.33$ m; μ_w = 0.018 kg mol^{-1}, R = 8.314 J mol^{-1} K^{-1}		$-0.097 \times \log(\psi/100) + 0.552$	
A.6 evapotranspiration						
A.6.1 canopy transpiration E_c	Penman-Monteith equation with sunlit and shaded leaf conductance	$(e_{c(T_c)} - e_a)/(r_c + r_a)$, e_s = canopy vapor concentration (g m^{-3}), e_a = atmospheric vapor concentration (g m^{-3}), r_a = aerodynamic resistance (s m^{-1}), $r_c = 0.64\, g_c^{-1}$	$(e_{s(T_c)} - e_a)/(r_c + r_a)$, e_s = saturated vapor concentration (g m^{-3}), e_a = atmospheric vapor concentration (g m^{-3}), r_a = aerodynamic resistance (s m^{-1}), $r_c = 0.64\, g_c^{-1}$	$(e_{s(T_c)} - e_a)/(r_c + r_a)$, e_s = saturated vapor concentration (g m^{-3}), e_a = atmospheric vapor concentration (g m^{-3}), r_a = aerodynamic resistance (s m^{-1}), $r_c = 0.64\, g_c^{-1}$	$(e_{s(T_c)} - e_l)/r_c$, e_s = saturated vapor concentration (g m^{-3}), e_a = vapor concentration at leaf surface (g m^{-3}), $r_c = 0.64\, g_c^{-1}$	$(e_{s(T_c)} - e_a)/(r_c + r_a)$, e_s = saturated vapor concentration (g m^{-3}), e_a = atmospheric vapor concentration (g m^{-3}), r_a = aerodynamic resistance (s m^{-1}), $r_c = 0.64\, g_c^{-1}$
A.6.2 canopy interception	Penman-Monteith equation with zero resistance	$(e_{s(T_c)} - e_a)/r_a$		$(e_{s(T_c)} - e_a)/r_a$	$(e_{s(T_c)} - e_a)/r_a$	$(e_{s(T_c)} - e_a)/r_a$
A.6.3 litter evaporation	Combined with soil	$(e_{l(T_l)} - e_a)/(r_a + r_b)$, $e_{l(T_l)}$ = vapor concentration at litter surface (g m^{-3}), r_b = aerodynamic resistance of plant canopy (s m^{-1})		Incorporated into soil surface evaporation	Treated as ground surface	Incorporated into soil surface evaporation
A.6.4 soil surface evaporation	Penman-Monteith equation with soil resistance	$(e_{s(T_s)} - e_a)/(r_a + r_b + r_l)$, $e_{s(T_s)}$ = soil surface vapor concentration (g m^{-3}), r_l = diffusive resistance of litter (s m^{-1})	$(e_{s(T_s)} - e_a)/r_a$, $e_{s(T_s)}$ = soil surface vapor concentration (g m^{-3})	Zero when stable, otherwise calculated from D at ground surface and free convection equation	$(e_{s(T_s)} - e_a)/(r_a + r_{ac})$, $e_{s(T_s)}$ = soil surface vapor concentration (g m^{-3}), r_{ac} = canopy modified r_a	=zero when stable, otherwise calculated from D at ground surface and free convection equation
A.6.5. soil water flow	Richards	Richards or Green-Ampt, Poiseuille, Manning	Richards	Richards	Richards	Richards

Appendix A (*Continued*)

	BEPS	*ecosys*	C-CLASSa	C-CLASSm	EALCO	CTEM
A.6.6 root water uptake	$= \Sigma_i(Tw_i)wi =$ $(R_i/\psi_i)/\Sigma_i(R_i/\psi_i)$, where T is the total transpiration; R_i is root fraction in layer i; and ψ_i is water potential in layer i	$\Sigma_i\{(\psi_c - \psi_s)/(\Omega_s + \Omega_r + \Sigma_x\Omega_{ax})\}$, equilibrated with E_c from A.6.1, ψ_c = canopy water potential (MPa), for each soil layer: ψ_s = soil water potential (MPa), Ω_s = soil hydraulic resistance (MPa h m^{-1}), Ω_r = root radial hydraulic resistance (MPa h m^{-1}), Ω_a = root axial hydraulic resistance (MPa h m^{-1})	$\Sigma_i\{(\psi_c - \psi_s)/(\Omega_s + \Omega_r)\}$, equilibrated with E_c, ψ_c = canopy water potential (m), for each soil layer: ψ_s = soil water potential (m), Ω_s = soil hydraulic resistance (s^{-1}), Ω_r = root hydraulic resistance (s^{-1})	Based on root fraction = $e^{(-3.0 \times \text{soil depth/max. root depth})}$ in each of 3 soil layers	$\Sigma_i\{(\psi_c - \psi_s)/(\Omega_s + \Omega_r + \Omega_{ax})\}$, ψ_c = canopy water potential (m), ψ_s = soil layer water potential (m), Ω_s = soil hydraulic resistance (s^{-1}), Ω_r = root radial hydraulic resistance (s^{-1}), Ω_{ax} = root axial hydraulic resistance (s^{-1})	Based on root fraction = $e^{(-3.0 \times \text{soil depth/max. root depth})}$ in each of 3 soil layers
A.6.7 soil profile resolution	4 layers: 0.10, 0.15, 0.35, and 1 m	User-selected layer numbers (15 max.) and depths, with surface layer typically 0.01 m	3 layers: 0.10, 0.25 and 3.75 m	3 layers: 0.10, 0.25 and 3.75 m	3 layers: 0.10, 0.25 and 1.15 m	3 layers: 0.10, 0.25 and 3.75 m

References

Amthor, J.S., Goulden, M.L., Munger, J.W., Wofsy, S.C., 1994. Testing a mechanistic model of forest-canopy mass and energy exchange using eddy correlation: carbon dioxide and ozone uptake by a mixed oak-maple stand. Aust. J. Plant Physiol. 21, 623–651.

Amthor, J.S., Chen, J.M., Clein, J., Frolking, S., Goulden, M.L., Grant, R.F., Kimball, J.S., King, A.W., McGuire, A.D., Nikolov, N.T., Potter, C.S., Wang, S., Wofsy, S.C., 2001. Boreal forest CO_2 exchange and evapotranspiration predicted by nine ecosystem process models: inter-model comparisons and relationships to field measurements. J. Geophys. Res. 106, 33623–33648.

Arain, M.A., Black, T.A., Barr, A.G., Jarvis, P.G., Massheder, J.M., Verseghy, D.L., Nesic, Z., 2002. Effects of seasonal and interannual climate variability on net ecosystem productivity of boreal deciduous and conifer forests. Can. J. For. Res. 32 (5), 878–891.

Arneth, A., Kelliher, F.M., McSeveny, T.M., Byers, J.N., 1998. Assessment of annual carbon exchange in a water-stressed *Pinus radiata* plantation: an analysis based on eddy covariance measurements and an integrated biophysical model. Global Change Biol. 5, 531–545.

Arora, V.K., 2003. Simulating energy and carbon fluxes over winter wheat using coupled land surface and terrestrial ecosystem models. Agric. For. Meteorol. 118 (1–2), 21–47.

Arora, V.K., Boer, G.J. 2003. A representation of variable root distribution in dynamic vegetation models. Earth Interactions 7, Paper 6, 19 pp.

Baldocchi, D.D., Wilson, K.B., 2001. Modelling CO_2 and water vapour exchange of a temperate broadeaved forest on daily to decadal time scales. Ecol. Model. 142, 155–184.

Baldocchi, D.D., Meyers, T.P., 1998. On using ecophysiological, micrometeorlogical and biochemical theory to evaluate carbon dioxide, water vapor and trace gas fluxes over vegetation: a perspective. Agric. For. Meteorol. 90, 1–25.

Ball, J.T., 1988. An analysis of stomatal conductance. Ph.D. Thesis, Stanford University, Stanford ,CA, 89 pp.

Barr, A.G., Griffis, T.J., Black, T.A., Lee, X., Staebler, R.M., Fuentes, J.D., Chen, Z., Morgenstern, K., 2002. Comparing the carbon budgets of boreal and temperate deciduous forest stands. Can. J. For. Res. 32, 813–822.

Bonan, G.B., 1991. A biophysical surface energy budget analysis of soil temperature in the boreal forests of interior Alaska. Water Resour. Res. 27 (5), 767–781.

Bowes, G., 1991. Growth at elevated CO_2: photosynthetic responses mediated through Rubisco. Plant Cell Environ. 14, 795–806.

Bunnell, F.L., Tait, D.E.N., Flanagan, P.W., van Cleve, K., 1977. Microbial respiration and substrate weight loss. I. A general model of the influence of abiotic variables. Soil Biol. Biochem. 9, 33–40.

Chen, J.M., Rich, P.M., Gower, S.T., Norman, J.M., Plummer, S., 1997. Leaf area index of boreal forests: theory, techniques, and measurements. J. Geophys. Res. 102, 29429–29443.

Chen, J.M., Liu, J., Cihlar, J., Goulden, M.L., 1999. Daily canopy photosynthesis model through temporal and spatial scaling for remote sensing applications. Ecol. Model. 124, 99–119.

Chen, W.J., Chen, J.M., Liu, J., Cihlar, J., 2000a. Approaches for reducing uncertainties in regional forest carbon balance. Global Biogeochem. Cycles 14, 827–838.

Chen, J.M., Chen, W., Liu, J., Cihlar, J., 2000b. Annual carbon balance of Canada's forests during 1895–1996. Global Biogeochem. Cycles 14, 839–850.

Chen, J.M., Ju, W., Cihlar, J., Price, D., Liu, J., Chen, W., Pan, J., Black, T.A., Barr, A., 2003. Spatial distribution of carbon sources and sinks in Canada's forests based on remote sensing. Tellus B. 55 (2), 622–642.

Collatz, G.J., Ball, J.T., Grivet, C., Berry, J.A., 1991. Physiological and environmental regulation of stomatal conductance, photosynthesis, and transpiration: a model that includes a laminar boundary layer. Agric. For. Meteorol. 54, 107–136.

Collatz, G.J., Ribas-Carbo, M., Berry, J.A., 1992. Coupled photosynthesis-stomatal conductance model for leaves of C4 plants. Aust. J. Plant Physiol. 19, 519–538.

Dang, Q.L., Margolis, H.A., Coyea, M.R., Sy, M., Collatz, G.J., 1997. Regulation of branch-level gas exchange of boreal trees: roles of shoot water potential and vapor pressure difference. Tree Physiol. 17, 521–535.

Doussan, C., Vercambre, G., Pagès, L., 1998. Modelling of the hydraulic architecture of root systems: An integrated approach to water absorption–distribution of axial and radial conductances in maize. Ann. Bot. 81, 225–232.

Drewitt, G.B., Black, T.A., Nesic, Z., Humphreys, E.R., Jork, E.M., Swanson, R., Ethier, G.J., Griffis, T., Morgenstern, K., 2002. Measuring forest floor CO_2 fluxes in a Douglas-fir forest. Agric. For. Meteorol. 110, 299–317.

Farquhar, G.D., von Caemmerer, S., Berry, J.A., 1980. A biochemical model of photosynthetic CO_2 assimilation in leaves of C_3 species. Planta 149, 78–90.

Gao, Q., Zhao, P., Zeng, X., Cai, X., Shen, W., 2002. A model of stomatal conductance to quantify the relationship between leaf transpiration, microclimate and soil water stress. Plant, Cell Environ. 25, 1373–1382.

Gower, S.T., Vogel, J.G., Stow, T.K., Norman, J.M., Kucharik, C.J., Steele, S.J., 1997. Carbon distribution and aboveground net-primary production in aspen, jack pine, and black spruce stands in Saskatchewan and Manitoba. Can. J. Geophys. Res. 102, 29,029–29,042.

Grant, R.F., 1998a. Simulation in *ecosys* of root growth response to contrasting soil water and nitrogen. Ecol. Model. 107, 237–264.

Grant, R.F., 2001. A review of the Canadian ecosystem model *ecosys*. In: Shaffer, M. (Ed.), Modeling Carbon and Nitrogen Dynamics for Soil Management. CRC Press, Boca Raton, FL, pp. 175–264.

Grant, R.F., 2003. Modelling topographic effects on net ecosystem productivity of boreal black spruce forests. Tree Physiol. 24, 1–18.

Grant, R.F., Oechel, W.C., Ping, C., Kwon, H., 2003. Carbon balance of coastal arctic tundra under changing climate. Global Change Biol. 9, 16–36.

Grant, R.F., Goulden, M.L., Wofsy, S.C., Berry, J.A., 2001a. Carbon and energy exchange by a black spruce – moss ecosystem under changing climate: testing the mathematical model *ecosys* with data from the BOREAS experiment. J. Geophys. Res. 106, 33,605–33,621.

Grant, R.F., Juma, N.G., Robertson, J.A., Izaurralde, R.C., McGill, W.B., 2001b. Long term changes in soil C under different fertilizer, manure and rotation: testing the mathematical model *ecosys* with data from the Breton Plots. Soil Sci. Soc. Am. J. 65, 205–214.

Grant, R.F., Wall, G.W., Kimball, B.A., Frumau, K.F.A., Pinter Jr., P.J., Hunsaker, D.J., Lamorte, R.L., 1999. Crop water relations under different CO_2 and irrigation: testing of ecosys with the free air CO_2 enrichment (FACE) experiment. Agric. For. Meteorol. 95, 27–51.

Grelle, A., Lindroth, A., Mölder, M., 1999. Seasonal variation of boreal forest surface conductance and evaporation. Agric. For. Meteorol. 98–99, 563–578.

Griffis, T.J., Black, T.A., Morgenstern, K., Barr, A.G., Nesic, Z., Drewitt, G.B., Gaumont-Guay, D., McCaughey, J.H., 2003. Ecophysiological controls on the carbon balances of three southern boreal forests. Agric. For. Meteorol. 117, 53–71.

Hanson, P.J., Amthor, J.S., Wullschleger, S.D., Wilson, K.B., Grant, R.F., Hartley, A., Hui, D., Hunt Jr., E.R., Johnson, D.W., Kimball, J.S., King, A.W., Luo, Y., McNulty, S.G., Sun, G., Thornton, P.E., Wang, S, Williams, M., Baldocchi, D.D., Cushmann, R.M., 2004. Oak forest carbon and water simulations: model intercomparisons and evaluations against independent data. Ecol. Monogr. 74, 443–489.

Humphreys, E.R., Black, T.A., Ethier, G.J., Drewitt, G.B., Spittlehouse, D.L., Jork, E.-M., Nesic, Z., Livingston, N.J., 2003. Annual and seasonal variability of sensible and latent heat fluxes above a coastal Douglas-fir forest, British Columbia. Can. Agric. For. Meteorol. 115, 109–125.

Hunt Jr., E.R., Lavigne, M.B., Franklin, S.E., 1999. Factors controlling the decline in net primary production with stand age for balsam fir in Newfoundland assessed using an ecosystem simulation model. Ecol. Model. 122, 151–164.

Jarvis, P.G., 1976. The interpretation of the variations in leaf water potential and stomatal conductance found in canopies in the field. Philos. Trans., R. Soc. Landon, Ser. B 273, 593–610.

Jarvis, P.G., Massheder, J.M., Hale, S.E., Moncrieff, J.B., Rayment, M., Scott, S.L., 1997. Seasonal variation in carbon dioxide, water vapor, and energy exchanges of a boreal black spruce forest. J. Geophys. Res. 102, 28,953–28,966.

Kellomäki, S., Wang, K.-Y., 1999. Short-term environmental controls of heat and water vapour fluxes above a boreal coniferous forest: model computations compared with measurements by eddy correlation. Ecol. Model. 124, 145–173.

Kellomäki, S., Wang, K.-Y., 2000. Short-term environmental controls on carbon dioxide flux in a boreal coniferous forest: model computation compared with measurements by eddy covariance. Ecol. Model. 128, 63–88.

Keyes, M.R., Grier, C.C., 1981. Above- and below-ground net production in 40-year-old Douglas-fir stands on low and high productivity sites. Can. J. For. Res. 11, 599–605.

Kimball, J.S., White, M.A., Running, S.W., 1997. BIOME-BGC simulations of stand hydrologic processes for BOREAS. J. Geophys. Res. 102, 29,043–29,051.

King, A.W., Post, W.M., Wullschleger, S.D., 1997. The potential response of terrestrial carbon storage to changes in climate and atmospheric CO_2. Climatic Change 35, 199–237.

Kloeppel, B.D., Gower, S.T., Vogel, J.G., Reich, P.B., 2000. Leaf-level resource use for evergreen and deciduous conifers along a resource availability gradient. Functional Ecol. 14 (3), 281–292.

Kothavala, Z., Arain, M.A., Black, T.A, Verseghy, D. Evaluating fluxes of energy, water vapour and carbon dioxide over common crops. Agric. For. Meteorol. Submitted for publication.

Landsberg, J.J., Waring, R.H., 1997. A generalized model of forest productivity using simplified concepts of radiation-use efficiency, carbon balance and partitioning. For. Ecol. Manage. 95, 209–228.

Law, B.E., Waring, R.H., Anthoni, P.M., Aber, J.D., 2000a. Measurements of gross and net ecosystem productivity and water vapour exchange of a *Pinus ponderosa* ecosystem, and an evaluation of two generalized models. Global Change Biol. 6, 155–168.

Law, B.E., Williams, M., Anthoni, P.M., Baldocchi, D.D., Unsworth, M.H., 2000b. Measuring and modelling seasonal variation of carbon dioxide and water vapour exchange of a *Pinus ponderosa* forest subject to soil water deficit. Global Change Biol. 6, 613–630.

Leuning, R., 1990. Modelling stomatal behavior and photosynthesis of Eucalyptus grandees. Aust. J. Plant Physiol. 17, 159–175.

Leuning, R., 1995. A critical appraisal of a combined stomatal-photosynthesis model for C3 plants. Plant Cell Environ. 18, 339–355.

Leuning, R., Kelliher, F.M., de Puree, D.G.G., Schulze, E.-D., 1995. Leaf nitrogen, photosynthesis, conductance and transpiration: scaling from leaves to canopies. Plant Cell Environ. 18, 1183–1200.

Liu, J., Chen, J.M., Cihlar, J., Park, W., 1997. A process-based boreal ecosystems productivity Simulator using remote sensing inputs. Remote Sens. Environ. 62, 158–175.

Liu, J., Chen, J.M., Cihlar, J., 2003. Mapping Evapotranspiration Based on Remote Sensing: An Application to Canada's Landmass. Water Resour. Res. 39, 1189–1200.

Menuccini, M., Grace, J., 1996. Hydraulic conductance, light interception and needle nutrient concentration in Scots pine stands and their relations with net primary productivity. Tree Physiol. 16, 459–468.

Méthy, M., Gillon, D., Houssard, C., 1997. Temperature-induced changes of photosystem II activity in *Quercus ilex* and *Pinus halepensis*. Can. J. For. Res. 27, 31–38.

Morgenstern, K., Black, T.A., Humphreys, E.R., Griffis, T.J., Drewitt, G.B., Cai, T., Nesic, Z., Spittlehouse, D.L., Livingstone, N.J., 2004a. Sensitivity and uncertainty in the carbon balance of a Pacific northwest Douglas fir forest during an El Niño/El Niña cycle. Agric. For. Meteorol. 123, 201–219.

Morgenstern, K., Nesic, Z., Black, T.A., 2004b. An intercomparison eddy-correlation system for the Fluxnet-Canada Research Network. In: Proceedings of 26th Conference on Agricultural and Forest Meteorology. American Meteorological Society, Vancouver, BC.

Nikolov, N.T., 1997. Mathematical modeling of seasonal biogeophysical interactions in forest ecosystems. Ph.D. Thesis. Colorado State Univ. Ft. Collins.

Ohta, T., Hiyama, T., Tanaka, H., Kuwada, T., Maximov, T.C., Ohata, T., Fukushima, Y., 2001. Seasonal variation in the energy and water exchanges above and below a larch forest in eastern Siberia. Hydrol. Proc. 15, 1459–1476.

Parton, W.J., Scurlock, J.M.O., Ojima, D.S., Gilmanov, T.G., Scholes, R.J., Schimel, D.S., Kirchner, T., Menaut, J-C., Seastedt, T., Garcia Moya, E., Kamnalrut, A., Kinyamario, J.I., 1993. Observations and modeling of biomass and soil organic matter dynamics for the grassland biome worldwide. Global Biogeochem. Cycles 7, 785–809.

Reichstein, M, Tenhunen, J.D., Roupsard, O., Ourcival, J.-M., Rambal, S., Miglietta, F., Peressotti, A., Pecchiari, M., Tirone, G., Valentini, R., 2002. Severe drought effects on ecosystem CO_2 and H_2O fluxes at three Mediterranean evergreen sites: revision of current hypotheses? Global Change Biol. 8, 99–1017.

Royce, E.B., Barbour, M.G., 2001. Mediterranean climate effects. I. Conifer water use across a Sierra Nevada ecotone. Am. J. Bot. 88, 911–918.

Ryan, M.G., Lavigne, M.B., Gower, S.T., 1997. Annual carbon cost of autotrophic respiration in boreal forest ecosystems in relation to species and climate. J. Geophys. Res. 104, 28871–28883.

Saugier, B., Granier, A., Pontailler, J.Y., Dufrêne, E., Baldocchi, D.D., 1997. Transpiration of a boreal pine forest measured by branch bag, sap flow and micrometeorological methods. Tree Physiol. 17, 511–519.

Sellers, P.J., Randall, A.A., Collatz, G.A., Berry, J.A., Field, C.B., Dazlich, D.A., Zhang, C., Collelo, G.D., Bounoua, L., 1996. A revised land surface parameterization (SiB2) for atmospheric GCMs Part I: model formulation. J. Clim. 9, 676–705.

Steele, S.J., Gower, S.T., Vogel, J.G., Norman, J.M., 1997. Root mass, net primary production and turnover in aspen, jack pine and black spruce forests in Saskatchewan and Manitoba. Can. Tree Physiol. 17, 577–587.

Stitt, M., 1991. Rising CO_2 levels and their potential significance for carbon flow in photosynthetic cells. Plant Cell Environ. 14, 741–762.

Twine, T.E., Kustas, W.P., Norman, J.M., Cook, D.R., Houser, P.R., Mayers, T.P., Prueger, J.H, Starks, P.J., Wesely, M.L., 2000. Correcting eddy-covariance flux underestimates over a grassland. Agric. For. Meteorol. 103, 279–300.

Verseghy, D.L., 2000. The Canadian Land Surface Scheme (CLASS): its history and future. Atmosphere-Ocean 38 (1), 1–13.

Verseghy, D.L., McFarlane, N.A., Lazare, M., 1993. CLASS – a Canadian land surface scheme for GCMS. II. Vegetation model and coupled runs. Int. J. Clim. 13, 347–370.

Wang, S.S., Grant, R.F., Verseghy, D.L., Black, T.A., 2001. Modelling plant carbon and nitrogen dynamics of a boreal aspen forest in CLASS – the Canadian Land Surface Scheme. Ecol. Model. 142, 135–155.

Wang, S.S., Grant, R.F., Verseghy, D.L., Black, T.A., 2002a. Modelling carbon dynamics of boreal forest ecosystems using the Canadian Land Surface Scheme. Clim. Change 55 (4), 451–477.

Wang, S.S., Grant, R.F., Verseghy, D.L., Black, T.A., 2002b. Modelling carbon-coupled energy and water dynamics of a boreal aspen forest in a general circulation model land surface scheme. Int. J. Clim. 22 (10), 1249–1265.

Wang, S., Leblanc, S., Fernandes, R., Cihlar, J., 2002c. Diurnal variation of direct and diffuse radiation and its impact on surface albedo. In: Proceedings of the 2002 IEEE International Geoscience and Remote Sensing Symposium and the 24th Canadian Symposium on Remote Sensing, Toronto, Canada.

Wang, S., Chen, W., Cihlar, J., 2002d. New calculation methods of diurnal distribution of solar radiation and its interception by canopy over complex terrain. Ecol. Model. 155, 191–204.

Wang, Y.P., Jarvis, P.G., 1990. Description and validation of an array model – MAESTRO. Agric. For. Meteorol. 51, 257–280.

Wang, Y.-P., Leuning, R., 1998. A two-leaf model for canopy conductance, photosynthesis and portioning of available energy. I. Model description and comparison with a multi-layered model. Agric. For. Meteorol. 91, 89–111.

Wesely, M.L., Hart, R.L., 1985. Variability of short term eddy-correlation estimates of mass exchange. In: Hutchinson, B.A., Hicks, B.B. (Eds.), The Forest–Atmosphere Interaction. D. Reidel, Dordrecht, pp. 591–612.

Williams, M., Rastetter, E.B., Fernandes, D.N., Goulden, M.L., Wofsy, S.C., Shaver, G.R., Mellilo, J.M., Munger, J.W., Fan, S.-M., Nadelhoffer, K.J., 1996. Modeling the soil-plant-atmosphere continuum in a Quercus-Acer stand at Harvard Forest: the regulation of stomatal conductance by light, nitrogen and soil/plant hydraulic properties. Plant Cell Environ. 19, 911–927.

Wilson, K., Baldocchi, D., 2000. Seasonal and interannual variability of energy fluxes over a broad-leaved temperate deciduous forest in North America. Agric. For. Meteorol. 100, 1–18.

Wullschleger, S.D., Gunderson, C.A., Tharp, L.M., West, D.C., 2003. Simulated patterns of forest succession and productivity as a consequence of altered precipitation. In: Hansen, P.J., Wullschleger, S.D. (Eds.), North American Temperate Deciduous Forest Responses to Changing Precipitation Regimes. Springer, New York, pp. 433–446.

Zhang, Y., Grant, R.F., Flanagan, L.B, Wang, S., Verseghy, D.L., 2004. Recent developments and testing of a carbon-coupled Canadian land surface scheme in a water-stressed northern temperate grassland. Ecol. Model. 181, 591–614.

Zierl, R., 2001. A water balance model to simulate drought in forested ecosystems and its application to the entire forested area in Switzerland. J. Hydrol. 242, 115–136.